Annu. Rev. Nucl. Part. Sci. 2000. 50:207–48


# PRECISION MEASUREMENTS OF THE *W* BOSON MASS

Douglas A. Glenzinski
*Enrico Fermi Institute, University of Chicago, Chicago, Illinois 60637, and Fermi National Accelerator Laboratory, Batavia, Illinois, 60510;*
*e-mail: Douglasg@fnal.gov*

Ulrich Heintz
*Physics Department, Boston University, Boston, Massachusetts 02215;*
*e-mail: heintz@bu.edu*



**Key Words** *W* boson, mass, precision, electroweak, Higgs boson

■ **Abstract** The standard model of electroweak interactions has had great success in describing the observed data over the past three decades. The precision of experimental measurements affords tests of the standard model at the quantum loop level beyond leading order. Despite this success, it is important to continue confronting experimental measurements with the standard model's predictions because any deviation would signal new physics. As a fundamental parameter of the standard model, the mass of the *W* boson, $M_W$, is of particular importance. Aside from being an important test of the model itself, a precision measurement of $M_W$ can be used to constrain the mass of the Higgs boson, $M_H$. In this article, we review the principal experimental techniques for determining $M_W$ and discuss their combination into a single precision $M_W$ measurement. We conclude by briefly discussing future prospects for precision measurements of the *W* boson mass.

## CONTENTS

# 1. INTRODUCTION

The standard model of electroweak interactions theoretically unites the electromagnetic and weak forces of nature. It postulates that these forces are communicated between the constituent particles of nature, quarks and leptons, by carriers known as gauge bosons. In particular, the electromagnetic force is carried by the photon, $\gamma$, while the weak force is mediated by the neutral $Z$ boson, $Z^0$, and the charged $W$ bosons, $W^{\pm}$. As such, the $W$ boson is fundamental to the standard model. Moreover, the mass of the $W$ boson, $M_W$, is a parameter of the theory itself, so that a comparison between the experimentally determined $M_W$ and the standard-model prediction provides an important and fundamental test of the theory. Alternatively, a precision measurement of $M_W$ can be used to estimate, within the framework of the standard model, other parameters, such as the mass of the Higgs boson, $M_H$.

## 1.1 Historical Overview

The weak force was first inferred from observations of nuclear $\beta$-decay, $n \rightarrow p + e^- + \overline{\nu}_e -$. In 1935, Fermi postulated the first theory of weak interactions. The form of the interaction was taken to be analogous with that of the electromagnetic interaction, and was characterized by a "coupling" (or strength) parameter—the Fermi constant, $G_F$. By comparing interaction rates, the strength of the weak force was estimated to be about $10^{-5}$ that of the electromagnetic force. Fermi's theory very successfully described low-energy weak interactions but violated unitarity at high energy.

In the 1960s Glashow, Weinberg, and Salam (1) proposed the electroweak $SU(2) \times U(1)$ gauge theory, which unifies the weak and electromagnetic forces. The theory postulated that the weak force is mediated by massive particles, the $W$ and $Z$ bosons, and predicted their masses to be of the order of 100 GeV.[1] The discovery of the $W$ boson in 1983, with a mass of $81 \pm 5$ GeV (2), was a great success for the electroweak theory. More rigorous tests of the theory require more precise determinations of the boson masses.

Over the past 15 years, a variety of experiments have measured the mass of the $W$ boson with ever-improving precision. The first measurements were made at the CERN $Sp\overline{p}S$ collider (3) by the UA1 (4) and UA2 (5) experiments. The UA2

[1] Throughout this article, we use units of $\hbar = c = 1$.

experiment made the first measurement of the $W$ boson mass at a relative precision below 1% (6). The CDF (7) and DØ (8) experiments at the Fermilab Tevatron (9), another $p\overline{p}$ collider, were the first to push the precision to the 0.1% level. More recently, measurements made at the CERN $e^+e^-$ collider, the Large Electron-Positron collider (LEP), by the ALEPH (10), DELPHI (11), L3 (12), and OPAL (13) experiments, have also reached relative precisions of 0.1%. Combining all these measurements yields a relative precision of 0.05% and affords stringent tests of the standard model. In particular, due to radiative corrections, such precision measurements offer indirect constraints on the mass of the Higgs boson.

## 1.2 The Electroweak Theory

In the $SU(2) \times U(1)$ electroweak theory, local gauge invariance is achieved by introducing four massless bosons, an isovector triplet $\mathbf{W}^\mu = (W_0^\mu, W_1^\mu, W_2^\mu)$, and an isosinglet, $B_0^\mu$. As in the electromagnetic case, the electroweak Lagrangian can be expressed as a product of currents and coupling parameters:

$$\mathcal{L} = g\mathbf{J}^\mu \cdot \mathbf{W}^\mu + g' J_Y^\mu B_0^\mu, \qquad 1.$$

where $\mathbf{J}^\mu$ and $J_Y^\mu$ are the weak isospin and hypercharge currents of the physical fermions (i.e. quarks and leptons), respectively, and $g$ and $g'$ are their couplings to the $\mathbf{W}^\mu$ and $B_0^\mu$ fields. The weak quantum numbers are related to the electric charge, $Q$, by $Q = I_3 + Y/2$, where $I_3$ is the third component of the weak isospin associated with the $SU(2)$ group and $Y$ is the weak hypercharge associated with the $U(1)$ group (more detailed discussions and derivations can be found, for example, in Reference 14). If the associated bosons were massless, the weak field would be a long-range (infinite) field, contradicting experimental evidence. This shortcoming can be addressed by imparting mass to the vector bosons, which is achieved by spontaneously breaking the $SU(2) \times U(1)$ symmetry with the introduction of an additional field. Demanding that the theory be valid to high energies and remain renormalizable, a necessary condition in order to extract meaningful theoretical predictions, constrains the form of this additional field. The simplest solution introduces a complex scalar isodoublet, the Higgs field, one component of which has a vacuum expectation value $v > 0$ (15). The physical boson fields can then be expressed as

$$W^\pm = (W_1 \pm W_2)/\sqrt{2}, \begin{pmatrix} Z^0 \\ A^0 \end{pmatrix} = \begin{pmatrix} \cos\theta_W & \sin\theta_W \\ -\sin\theta_W & \cos\theta_W \end{pmatrix} \begin{pmatrix} B_0 \\ W_0 \end{pmatrix} \qquad 2.$$

for the charged $W$ bosons, $W^\pm$, the neutral $Z$ boson, $Z^0$, and the photon, $A^0$, respectively. The weak mixing angle, $\theta_W$, relates the $SU(2)$ and $U(1)$ coupling constants to the electromagnetic coupling constant (i.e. the fine structure constant), $\alpha$, by

$$g^2 = 4\pi\alpha/\sin^2\theta_W, \quad g'^2 = 4\pi\alpha/\cos^2\theta_W. \qquad 3.$$

The gauge boson masses are given by

$$M_W = gv/2,\ M_Z = v\sqrt{g^2 + g'^2}/2,\ M_A = 0, \quad 4.$$

corresponding to the massive $W^{\pm}$ and $Z^0$ bosons and the massless photon, respectively. Equations 3 and 4 yield the following relationship: $\sin^2\theta_W = 1 - (M_W/M_Z)^2$.

At low energies, the electroweak theory is equivalent to the Fermi theory of weak interactions. Comparing the electroweak Lagrangian in Equation 1 to Fermi's expression for the weak interaction yields the following equality: $G_F = g^2/(4\sqrt{2}M_W^2) = \pi\alpha/(\sqrt{2}M_W^2 \sin^2\theta_W)$. This can be rewritten as

$$M_W^2\left(1 - \frac{M_W^2}{M_Z^2}\right) = \frac{\pi\alpha}{\sqrt{2}G_F}, \quad 5.$$

relating the mass of the $W$ boson, the mass of the $Z$ boson, the fine structure constant, and the Fermi constant, so that a measurement of three yields a prediction of the fourth. To obtain theoretical predictions of a precision comparable to that of the experimental determinations of these parameters, radiative corrections must be included. These corrections can be incorporated by rewriting Equation 5 as

$$M_W^2\left(1 - \frac{M_W^2}{M_Z^2}\right) = \frac{\pi\alpha}{\sqrt{2}G_F}\left(\frac{1}{1-\Delta r}\right), \quad 6.$$

where the effects of the radiative corrections are included in the additional term, $\Delta r$. The corrections can be separated into three main pieces,

$$\Delta r = \Delta\alpha + \Delta\rho\left(m_{\text{top}}^2\right) + \Delta\chi(\ln(M_H/M_Z)), \quad 7.$$

which include the running of the fine structure constant, $\Delta\alpha$, a quadratic dependence on the top quark mass, $\Delta\rho$, and a logarithmic dependence on the mass of the Higgs boson, $\Delta\chi$ (see Reference 16, for example, for a more detailed discussion and review of electroweak radiative corrections). This last dependence is a unique consequence of the non-Abelian gauge structure of the electroweak theory, which allows interactions among the gauge bosons themselves. It is because of these radiative corrections that precision measurements of $G_F$, $\alpha$, $M_Z$, and $M_W$, when compared with theoretical calculations, can yield constraints on $m_{\text{top}}$ and $M_H$ (see Reference 17 for a more detailed discussion and historical perspective).



## 2. MEASUREMENTS OF $M_W$ AT $p\bar{p}$ COLLIDERS

### 2.1 Measurement Techniques

#### 2.1.1 *W* Boson Production

Two $p\bar{p}$ colliders have had sufficient center-of-mass energy ($\sqrt{s}$) to produce $W$ bosons: the $Sp\bar{p}S$ at CERN ($\sqrt{s} = 630$ GeV) and the Tevatron at Fermilab ($\sqrt{s} = 1.8$ TeV). Figure 1 shows the most important subprocesses for $W$ boson production in $p\bar{p}$ collisions. At these center-of-mass energies, the dominant

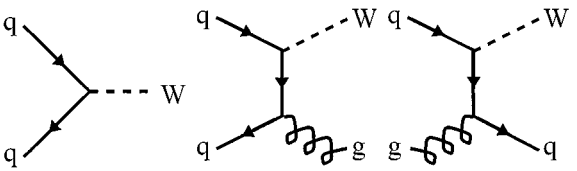


**Figure 1** Feynman diagrams for *W* boson production in $p\overline{p}$ collisions.



subprocess is $q\overline{q} \rightarrow W$. *Z* bosons, which form an essential control sample, are produced via analogous processes.

The *W* boson mass measurements from these colliders all make use of the $W \rightarrow e\overline{\nu}$ and $W \rightarrow \mu\overline{\nu}$ decay channels. *Z* bosons are identified by their decays to $e^+e^-$ or $\mu^+\mu^-$. Electrons and muons[2] are easy to trigger on and their momenta can be measured very precisely. Moreover, *W* and *Z* bosons are the dominant source of isolated, high-$p_T$ electrons and muons in $p\overline{p}$ collisions. Therefore, samples of *W* and *Z* decays involving electrons and muons can be identified with very little background. Purely hadronic decays of the *W* boson are swamped by QCD background. Decays involving $\tau$ leptons are difficult to identify because the $\tau$ leptons decay before they enter the detector.

The cross sections for *W* and *Z* production in $p\overline{p}$ collisions are large, $\sigma \times \mathcal{B} =$ 680 pb at $\sqrt{s} = 630$ GeV (18) and 2.3 nb at $\sqrt{s} = 1.8$ TeV (19) for *W* bosons, where $\mathcal{B}$ is the leptonic branching fraction. For *Z* bosons the corresponding values are about 10 times smaller.

In the following, we refer to a coordinate system that has its origin at the average $p\overline{p}$ collision point. The *z*-axis is defined by the proton beam. The *y*-axis points up. The *x*-axis points along the horizontal. Since the parton center-of-mass frame is boosted along the beam direction, momentum components transverse to the beam are especially important. They are denoted by a subscript *T*. The beams are unpolarized, resulting in an inherent azimuthal symmetry. Thus, it is often convenient to work in a cylindrical coordinate system in which $\phi$ is the angle relative to the *x*-axis in the *x*-*y* plane. The longitudinal phase space is most conveniently expressed in terms of the pseudorapidity, $\eta = -\ln \tan(\theta/2)$, which is related to the polar angle $\theta$.

The detectors have approximate azimuthal and forward-backward symmetry. They are constructed to cover as large a region as possible in pseudorapidity. From inside out, they typically consist of several subdetectors: a tracking system to measure the trajectories of charged particles; a calorimeter to measure the energy of electrons, photons, and hadrons; and a muon detection system. The tracking system may be located in a magnetic field to determine the momentum of charged particles from the curvature of their trajectories.

[2]Throughout this article, charge conjugation is implied.

### 2.1.2 Event Characteristics

The detectors register the charged lepton from the decay of the $W$ boson, while the neutrino escapes detection. The initial proton and antiproton break up in the collision and the fragments hadronize, contributing additional particles to the event. The hadronization of final-state quarks or gluons also contributes particles, which may form jets if the initial parton had sufficient transverse momentum. We refer to all particles, except the $W$ boson and its decay products, as the underlying event. Some of the particles of the underlying event escape through the beam pipe and are not detected at all. These particles may carry a substantial momentum component along the beam axis, but they carry little momentum transverse to the beam.

The transverse momenta of all final-state particles must add to zero, because the initial $p\overline{p}$ momentum is zero and momentum is conserved. Since the undetected neutrino carries away substantial momentum, the transverse momenta of all observed final-state particles do not add to zero. The apparent transverse momentum imbalance is called "missing $p_T$."

The particles of the underlying event that fall within the detector acceptance cannot all be detected individually. The detector measures the sum of the energy of all particles incident on one calorimeter segment. The quantity

$$\vec{u}_T = \sum_i E_i \sin\theta_i \hat{\imath} \qquad 8.$$

gives an approximate measurement of the total transverse momentum of all underlying event particles. The sum runs over all calorimeter cells, except those assigned to the charged lepton. $E_i$ is the energy in cell $i$. The unit vector $\hat{\imath}$ forms a right angle with the beam axis and points from the beam to cell $i$.

Thus, the basic observables are the momentum of the charged lepton ($\vec{p}^{\,\ell}$, $\ell = e$ or $\mu$) and the sum of the transverse momenta of the particles in the underlying event ($\vec{u}_T$), which we call the recoil momentum. From these observables, the transverse momenta of the $W$ boson ($\vec{p}_T^{\,W} = -\vec{u}_T$) and the neutrino ($\vec{p}_T^{\,\nu} = -\vec{u}_T - \vec{p}_T^{\,\ell}$) can be inferred. A high-$p_T$ charged lepton and large missing $p_T$ form the characteristic signature of $W$ boson decay events. $Z$ decay events are characterized by two charged leptons with high $p_T$. There are no high-$p_T$ neutrinos in such $Z$ decays and therefore no significant missing $p_T$ is expected.

### 2.1.3 Mass Measurement Method

It is not possible to reconstruct the invariant mass of the $W$ boson because there is no measurement of the momentum component of the neutrino along the beam axis. In addition, the $W$ bosons are not produced at rest, nor are they the only particles produced in the collisions. Therefore, a precision measurement of the $W$ boson mass using $W$ bosons produced in $p\overline{p}$ collisions poses a particular challenge.

The most precise measurements of the mass of the $W$ boson are based on the transverse mass of the charged lepton-neutrino pair, defined as

$$m_T = \sqrt{2p_T^\ell p_T^\nu (1 - \cos(\phi^\ell - \phi^\nu))}. \quad 9.$$

The advantage of the transverse mass is its invariance under boosts along the beam axis. Boosts transverse to the beam axis only give rise to corrections of the order of $(p_T^W/E^W)^2$. On the other hand, the transverse mass depends on the measurement of the recoil momentum $\vec{u}_T$ and all the associated systematic effects.

An alternative method to determine $M_W$ uses the $p_T$ spectrum of the lepton. This has the advantage of being insensitive to $u_T$. However, it is affected by the boost of the $W$ boson transverse to the beam axis to order $p_T^W/E^W$ and is therefore much more sensitive to systematic effects associated with the production of the $W$ bosons.

In principle, the charged lepton momentum or the transverse momentum of the neutrino can also be used to measure the $W$ boson mass. However, the former is sensitive to boosts in all directions and the latter suffers from poor resolution. These variables serve mainly as cross checks.

It is not possible to describe analytically the spectra of the variables mentioned above. They must be calculated numerically using a Monte Carlo model that takes into account the mechanisms for production and decay of $W$ bosons, as well as detector effects.

### 2.1.4 Backgrounds

The backgrounds to the $W \to \ell\overline{\nu}$ signal are $W \to \tau\overline{\nu} \to \ell\overline{\nu}\overline{\nu}\nu$ (1–2%), hadronic backgrounds (1% for $W \to e\overline{\nu}$, $\ll$1% for $W \to \mu\overline{\nu}$), $Z \to \ell^+\ell^-$ ($\ll$1% for $W \to e\overline{\nu}$, 4% for $W \to \mu\overline{\nu}$), and cosmic rays ($\ll$1%). Hadronic backgrounds arise from jet production in $p\overline{p}$ collisions if one of the jets fakes the charged lepton signature. $Z \to \ell^+\ell^-$ decays can enter the $W$ sample if one of the leptons escapes detection. The quoted percentages give the approximate residual fractions of background events in the final $W$ samples. The precise background contamination depends on the details of the event selection and the detector. They have to be taken into account in the measurement to avoid biasing the result. The normalization and shapes of the background spectra are determined from control data samples and detailed Monte Carlo simulations.

### 2.1.5 Event Selection

The event selection consists of the identification of the charged lepton and a set of kinematic and topological cuts. The selection criteria have to achieve two competing goals: to reject backgrounds efficiently and to minimize any biases to the selected event sample. Kinematic cuts, requiring the momentum of the charged lepton and missing $p_T$ above a threshold (typically 25 GeV), are easy to simulate and reduce backgrounds significantly. $W$ bosons with very high

transverse momenta do not add to the statistical significance of the mass measurement because their transverse mass and lepton $p_T$ spectra are very broad and carry little mass information. In addition, their recoil response is difficult to simulate and they are subject to higher background contamination. Thus, such events are usually eliminated from the sample by the requirement that the $W$ boson $p_T$ is below some threshold and/or that there are no high-$p_T$ jets in the events.

An electron is typically identified as an energy deposit in the calorimeter, consistent in shape with an electromagnetic shower, and a track that points to it. Since these electrons are highly relativistic, their momenta can be equated to the energy measured in the calorimeter. A muon is typically identified as a track stub in the muon detection system that matches a track in the tracking system and energy deposits in the calorimeter, small enough to be consistent with the passage of a minimum-ionizing particle. These criteria reduce contamination from hadronic backgrounds. However, both criteria inherently require the lepton to be isolated from other activity in the event. This biases the selection toward event topologies in which the charged lepton is emitted along the direction of motion of the $W$ boson. In such events, the probability is smaller that the lepton overlaps with a recoil particle. Since the boost of the $W$ boson increases the lepton $p_T$ in the lab frame, these events tend to have higher-momentum charged leptons and lower momentum neutrinos. This bias does not affect the transverse mass spectrum significantly, but it must be understood to predict the $p_T$ spectra of the charged leptons and the neutrinos correctly.

Specific cuts are required to reject events caused by an accidental coincidence between a cosmic ray traversing the detector and a beam crossing.

### 2.1.6 Monte Carlo Model

This section gives a generic description of the Monte Carlo models. The following sections describe the individual measurements and highlight significant experiment-specific differences. To keep statistical fluctuations negligible in the Monte Carlo simulation, it is necessary to generate many millions of $W$ decay events. To simulate such large event samples, parameterized Monte Carlo algorithms for $W$ boson production and decay and detector modeling were developed specifically for the $W$ mass measurements.

First, the $W$ bosons are generated. Their $p_T$ distribution is determined theoretically (from QCD-based calculations), empirically (from the observed $p_T$ distribution of $Z$ bosons), or both. The rapidity distribution of the generated $W$ bosons depends on the momentum distribution of the partons inside the proton. To determine it, a specific set of parton distribution functions must be chosen. The mass distribution of the generated $W$ bosons is a relativistic Breit-Wigner curve with its peak at the hypothesized value of the $W$ boson mass and an $s$-dependent width, given by the standard-model prediction. This mass spectrum is skewed

toward lower mass values by the momentum distribution of the partons inside the proton.

Next, the $W$ bosons are allowed to decay. At lowest order, the angular distribution of the charged leptons is $d\sigma/d\cos\theta^* \propto (1-\xi q\cos\theta^*)^2$, where $\theta^*$ is the scattering angle of the charged lepton in the rest frame of the $W$ boson, $q$ is the charge of the lepton, and $\xi$ is the helicity of the $W$ boson. In most events the initial quark originates from the proton and $\xi$ equals $-1$. In the much less likely case that the initial antiquark comes from the proton, $\xi$ equals $+1$. Higher-order QCD processes modify the angular distribution of the leptons. Radiative decays, $W\to\ell\overline{\nu}\gamma$, modify the momentum spectrum of the leptons. Either the Monte Carlo models include these effects or corrections are applied to the results.

The decay $W\to\tau\overline{\nu}\to\ell\overline{\nu}\nu\nu$ leads to events that are topologically indistinguishable from $W\to\ell\overline{\nu}$. Their rate can be calculated precisely in the framework of the standard model and they are typically included in the Monte Carlo model.

Finally, the Monte Carlo simulation must account for detector effects. The simulation starts out with the "true" momenta of the $W$ boson (and thus the recoil momentum) and the charged lepton in the event. These momenta are modified to account for experimental resolutions, biases, and efficiencies. Adding random Gaussian uncertainties to the observables simulates resolution effects. The widths of these Gaussian distributions are parameterized in detector-specific ways. Other effects accounted for include the response of the detector to the charged lepton and to the underlying event. Also modeled are the partial overlap of energy deposits of the lepton and underlying event, which leads to biases in lepton and recoil momentum measurements, and selection efficiencies that depend on kinematics or topology of the events.

Events due to the process $p\overline{p}\to Z+X$, $Z\to\ell^+\ell^-$ constitute an extremely important control sample to determine these effects. Comparing the observed $Z$ peak to the known $Z$ boson mass calibrates the energy or momentum response to charged leptons. The observed width of the $Z$ peak measures the energy or momentum resolution for charged leptons. The $Z$ boson $p_T$ can be measured directly using the charged leptons from its decay and indirectly from the recoil momentum. By comparing both determinations, the $Z$ events also serve to calibrate the recoil momentum response of the detector relative to the charged lepton response.

### 2.1.7 Mass Measurement

The Monte Carlo model predicts the shape of the transverse mass and the lepton $p_T$ spectra from $W\to\ell\overline{\nu}$ decays as a function of the assumed value of the $W$ boson mass. These spectra are added to the estimated background spectra and normalized to obtain probability density functions for a maximum likelihood fit to the spectra from the collider data. The statistical uncertainty in the fit to the $m_T$ spectrum is typically 11 GeV/(number of events)$^{1/2}$.

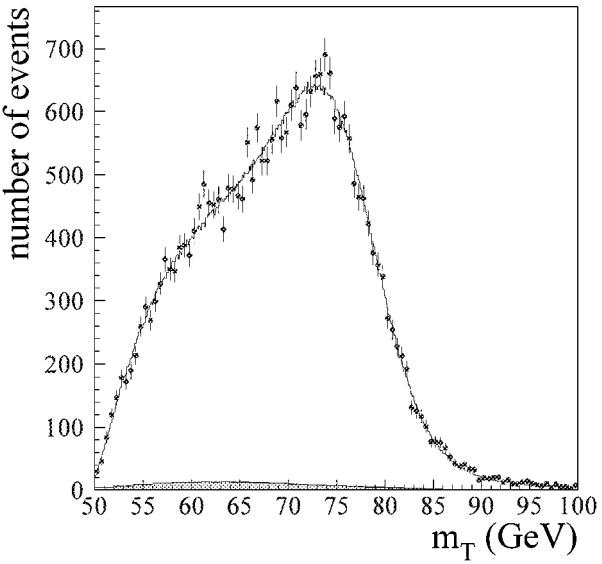


**Figure 2** Transverse-mass spectrum from *W* decay measured by DØ (20).



Figures 2 and 3 show representative spectra of transverse mass and lepton $p_T$. These spectra were measured by the DØ experiment. The points indicate the collider data, the line indicates the Monte Carlo prediction that agrees best with the data, and the small shaded region indicates the estimated background contribution.

### 2.1.8 Systematic Uncertainties

All inputs to the Monte Carlo model contribute to the systematic uncertainty of the measurement of the *W* boson mass. Each such uncertainty is estimated by varying the input parameter within its 68% confidence interval. The total systematic uncertainty is the sum in quadrature of all such contributions. Most of the model parameters are constrained by control data samples, most notably by the $Z \to \ell^+\ell^-$ samples. In most cases, the precision with which these parameters can be determined is limited by the size of the control samples, so that these uncertainties are really statistical in nature. This means that they can be quantified in a well-defined way. There are some cases in which no rigorous confidence interval can be defined, as is more typical of systematic uncertainties.

The following paragraphs elaborate on the most important categories of systematic uncertainties. The values quoted for each uncertainty are typical of the measurements from the Tevatron using a fit to the $m_T$ spectrum from a data sample of about 100 $\text{pb}^{-1}$.

***Lepton Energy/Momentum Scale (70–85 MeV)*** The uncertainty in the lepton energy/momentum scale is the most important systematic effect. Since all detector

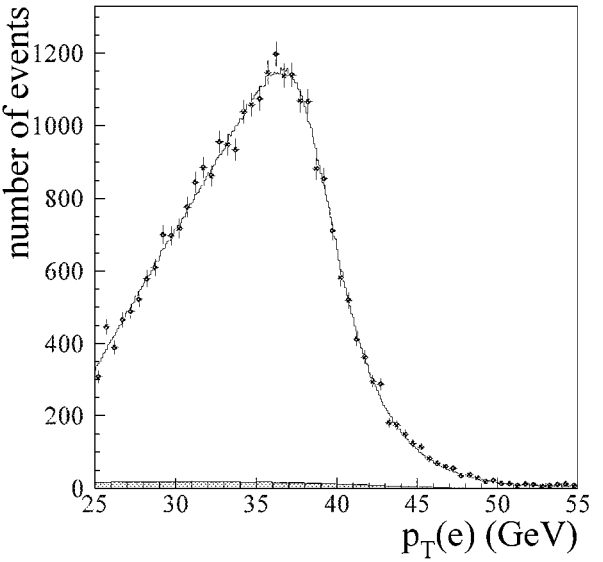


**Figure 3** Electron $p_T$ spectrum from *W* decays measured by DØ (20).



responses are calibrated against the charged leptons using the *Z* sample, the measured *W* mass simply scales with the lepton scale. It can be set in two ways.

One method is to calibrate the lepton scale so that the $Z \to e^+e^-$ and $Z \to \mu^+\mu^-$ mass peaks (Figure 4) agree with the known *Z* boson mass (21). An advantage of this method is that the uncertainty is dominated by statistical fluctuations in the *Z* sample, approximately 3 GeV/(number of events)$^{1/2}$, and little extrapolation is needed to the energies of leptons from *W* decays. Uncertainties in the extrapolation can be limited by using other resonances, such as $J/\psi \to e^+e^-$ or $\pi^0 \to \gamma\gamma$. If the scale calibration of the charged leptons is tied to the *Z* boson mass, the measured quantity is really the ratio of the *W* and *Z* boson masses, rather than the *W* boson mass. Of course, given that the *Z* boson mass is known so precisely, the two quantities are de facto equivalent.

Detectors with a magnetic tracking system can alternatively calibrate the momentum measurement for charged tracks, using for example $J/\psi \to \mu^+\mu^-$ decays (Figure 5), and then extrapolate to the momentum of leptons from *W* decays. The calorimeter must then be calibrated against the track momentum using the ratios of energy and momentum ($E/p$) measured for electrons from *W* decays. The advantage of the latter method lies in the higher precision of the track momentum calibration. Its disadvantages are the systematic effects associated with the extrapolation to higher momenta and the effects of radiation on the $E/p$ spectrum.

***Lepton Energy/Momentum Resolution (20–25 MeV)*** The electron energy resolution can be modeled as $\sigma/E = (\mathcal{S}^2/E + \mathcal{C}^2)^{1/2}$, where $E$ is the electron energy,

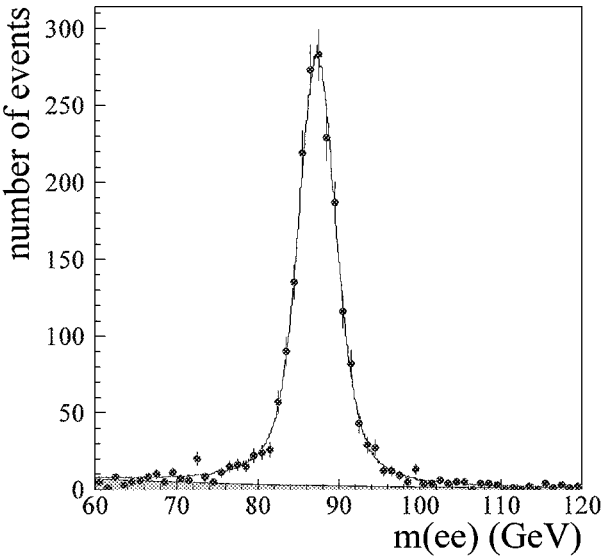


**Figure 4** Mass spectrum from $Z \rightarrow e^+e^-$ decays measured by DØ (20).

$\mathcal{S}$ is the sampling term, and $\mathcal{C}$ is the constant term. The value of $\mathcal{S}$ is taken from beam tests and $\mathcal{C}$ is chosen so that the width of the $Z$ peak predicted by the Monte Carlo model agrees with the $Z$ peak from collider data. For muons, the transverse momentum resolution is of the form $\sigma / p_T^2 = \kappa$, where $p_T$ is the transverse momentum of the muon and $\kappa$ is a constant chosen to match the widths of the $Z$ peaks from the Monte Carlo model and the collider data.

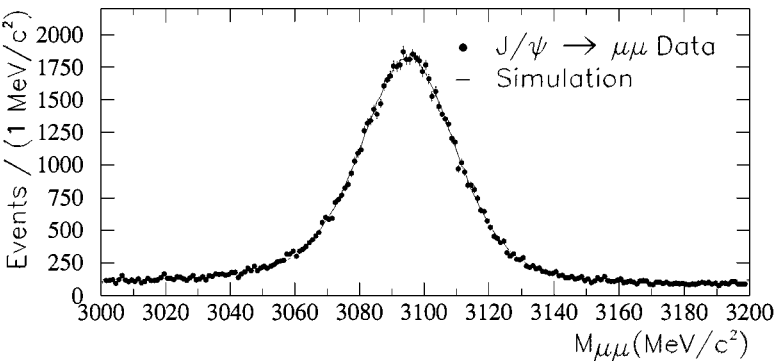


**Figure 5** Mass spectrum from $J/\psi \rightarrow \mu^+\mu^-$ decays measured by CDF (22).

***Recoil Model (30–40 MeV)*** The uncertainty in the recoil model arises from the parameters describing the response and resolution of the detector to the underlying event. These effects are determined from $Z$ decays and to a lesser extent from $W$ decays.

***Lepton Removal (≈15 MeV)*** The uncertainties in the corrections to the recoil momentum arise from the imperfect separation of energy deposits between the charged lepton and underlying event. Some particles from the underlying event inevitably overlap with the charged lepton in the calorimeter. Their energies are not included in the calculation of $u_T$. The correction is equal to the average energy deposited by the underlying event in an appropriately sized calorimeter segment in the $W$ data sample.

***Proton Structure (10–20 MeV)*** The uncertainty in the proton structure is characterized by the variations in the result for different choices of parton distribution functions. Though relatively small, this uncertainty is completely common to all measurements at $p\overline{p}$ colliders. For any given set of parton distribution functions, the variation in the measured $W$ boson mass is strongly correlated with the variation in the predicted forward-backward charge asymmetry in $p\overline{p} \rightarrow W \rightarrow \ell\overline{\nu}$ (22). Recently, increasingly precise measurements of this asymmetry by the CDF collaboration (23, 24) have helped constrain the parton distribution functions (e.g. 25, 26) and reduce the resulting uncertainty in the $W$ boson mass measurement. The agreement of recent parton distribution functions with the measured asymmetry is shown in Figure 6. Since complete error matrices are not available for parton distribution functions, this uncertainty cannot be evaluated in a statistically rigorous fashion.

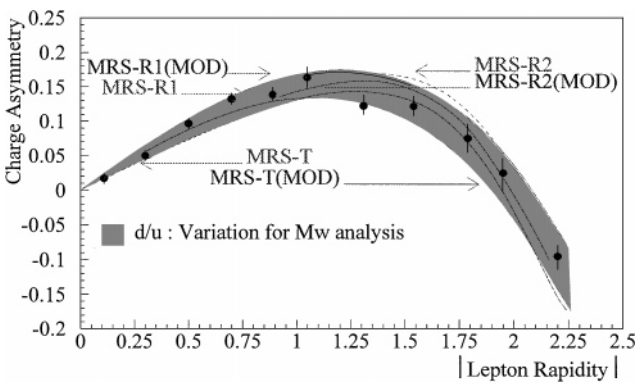


**Figure 6** Charge asymmetry in $p\overline{p} \rightarrow W \rightarrow \ell\overline{\nu}$ measured by CDF (24), compared with predictions of different parton distribution functions.

***W $p_T$ Spectrum (≈10 MeV)*** The shape of the $W$ $p_T$ distribution can be constrained by theoretical calculations in conjunction with the observed $Z$ $p_T$ distribution. For low $p_T$, the $W$ $p_T$ spectrum cannot be calculated perturbatively. One approach (27, 28) uses the Collins-Soper-Sterman resummation formalism (29, 30), which contains universal empirical parameters. These parameters can be constrained by requiring the calculation to agree with the observed $Z$ $p_T$ spectrum. Another, essentially equivalent, approach is to use the observed $Z$ $p_T$ spectrum directly and convert it to a prediction for the $W$ $p_T$ spectrum using the ratio of the calculated $W$ and $Z$ $p_T$ spectra. The precision of both approaches is limited by statistical fluctuations in the $Z$ data sample. The measured $W$ $p_T$ spectrum does not provide a very stringent constraint because its shape at low $p_T$ is dominated by the recoil response of the detector. The $Z$ $p_T$ spectrum, on the other hand, can be measured independently of the recoil response using the two charged leptons from the decay of the $Z$.

***Higher-Order Corrections (10–20 MeV)*** Calculations of radiative $W$ boson decays involving one photon (31, 32) and two photons (33) are available. The precision of these corrections is limited by experimental factors that determine the separation of the photons and the lepton in the calorimeter.

***Backgrounds (5–25 MeV)*** The hadronic background dominates this uncertainty for the $W \to e\overline{\nu}$ channel. Normalization and shape are determined from control data samples. The $Z \to \mu^+\mu^-$ decay dominates the background to the $W \to \mu\overline{\nu}$ channel. Uncertainties in the tracking efficiency at high $|\eta|$ and in the parton distribution functions are important contributions to this uncertainty.

## 2.2 Individual Measurements

### 2.2.1 UA2 Experiment

The UA2 collaboration published the first measurement of the $W$ Boson mass with a precision below 1% (6). This was superseded by an improved result (34) based on 13 pb$^{-1}$ of data taken in 1988–1990 at the CERN $Sp\overline{p}S$ collider at $\sqrt{s} = 630$ GeV.

The calorimeter of the UA2 detector (5) covers the pseudorapidity range $|\eta| < 3$. It consists of lead and iron absorber plates interspersed with scintillators and wavelength shifter readout. The electromagnetic section is 17–24 radiation lengths deep and is segmented into elements covering 15° in azimuth and approximately 0.2 units in pseudorapidity. The electron energy resolution is $\sigma/E = 17\%/\sqrt{E/\text{GeV}}$. The hadronic section is four interaction lengths deep. Inside the calorimeter are nested cylindrical tracking detectors. From inside out, they are as follows: a drift chamber with arrays of silicon pad counters on either side, a transition radiation detector, and a scintillating fiber detector. The detector has no magnetic field.

The $W$ boson mass measurement uses the $W \to e\overline{\nu}$ and $Z \to e^+e^-$ decay channels. The selection for the $W$ event sample requires an electron in the central calorimeter, $p_T^e > 20$ GeV, $p_T^\nu > 20$ GeV, $u_T < 20$ GeV, and $40 < m_T < 120$ GeV.

The Monte Carlo model calculates the $W$ boson rapidity from HRMSB structure functions (35). The spectrum of $p_T^W$ is taken from a calculation (28), modified by an empirical distortion function. The distortion function is determined by comparing the spectrum of $p_T^Z$ predicted by the same calculation with the observed $p_T^Z$ distribution. The recoil response model has two parameters: resolution (dependent on the total energy measured in the event) and offset (dependent on $p_T^W$). Both were tuned using the $Z \to e^+e^-$ sample and requiring that the mean $p_T^W$ predicted by the model agrees with the data.

Two $Z$ samples are used. Sample 1 requires two central electrons, which must be inside the fiducial volume of the calorimeter within $|\eta| < 0.8$. Sample 2 requires one central electron and one electron outside the central acceptance region. The energy of the "outside" electron is rescaled so that all transverse momentum components along the outer bisector of the two electron directions add to zero.

A fit to the transverse mass spectrum gives $80.84 \pm 0.22 \pm 0.83$ GeV. [3] The $Z$ mass measurement from both $Z$ samples is $91.74 \pm 0.28 \pm 0.93$ GeV. In all cases, the systematic uncertainties are dominated by the electron energy scale calibration. In the ratio $M_W/M_Z$, the energy scale and other systematic uncertainties partially cancel. UA2 finds $M_W/M_Z = 0.8813 \pm 0.0036 \pm 0.0019$. Using the current $Z$ mass of $91.187 \pm 0.002$ GeV (21) gives $M_W = 80.36 \pm 0.33 \pm 0.17$ GeV. [4]

### 2.2.2 CDF Experiment

The CDF collaboration has measured the $W$ boson mass using data sets from three running periods of the Fermilab Tevatron: 1988/1989 (36), 1992/1993 (22), and 1994–1996 (37). A publication of the results from the 1994–1996 data is in preparation.

The CDF detector (7, 38) is a multipurpose magnetic spectrometer. Tracking detectors are surrounded by a solenoid that provides an axial magnetic field of 1.4 T. The vertex time-projection chamber measures the position of the $p\overline{p}$ collision point along the $z$-axis with 1 mm resolution. The central tracking chamber has 84 layers of wires and covers $40^\circ < \theta < 140^\circ$. The transverse momentum resolution is $\sigma/p_T^2 = 0.0011/\text{GeV}$.

The central calorimeter covers $|\eta| < 1.1$. The electromagnetic section consists of lead plates interleaved with scintillator. Including chamber wall and solenoid, it is 19 radiation lengths deep and segmented into projective towers covering $\Delta\phi \times \Delta\eta = 15^\circ \times 0.1$. The electron energy resolution is $\sigma = 13.5\%\sqrt{E \sin\theta/\text{GeV}}$. Proportional chambers after 6 radiation lengths measure the shower centroid position to 3 mm. The hadron calorimeter is made of iron-scintillator shower counters. Outside the central region ($1.1 < |\eta| < 4.2$), the calorimeter is made of gas proportional chambers with cathode pad readout.

[3] Whenever two uncertainties are given, the first is due to statistical fluctuation, the second to systematic effects.

[4] Updated relative to original publication.

Muon chambers are located 3.5 m from the beam behind 5 nuclear absorption lengths of material and cover $|\eta| < 0.6$.

CDF measures both the $W \to e\overline{\nu}$ and $W \to \mu\overline{\nu}$ decay channels. Events are selected with $p_T^{\ell} > 25$ GeV and $p_T^{\nu} > 25$ GeV. There must be no high-$p_T$ tracks or energetic clusters in the calorimeter in addition to the charged lepton. For the 1992/1993 data sample, $u_T < 20$ GeV is required.

The muon momentum scale is based on a calibration of the tracking system to the $J/\psi$ mass. The electron energy scale is set using $E/p$ for electrons from $W$ decays. The calibration is checked using the reconstructed $Z$ mass from $Z \to e^+e^-$ decays, $91.12 \pm 0.52$ GeV (1988/1989) and $90.88 \pm 0.19 \pm 0.20$ GeV (1992/93), based on the same calibration as for $W \to e\overline{\nu}$ events.

In the analysis of the 1994–1996 data, the electron energy scale determined by the $E/p$ technique results in a reconstructed $Z$ mass peak from $Z \to e^+e^-$ decays that is 3.9 standard deviations below the nominal $Z$ mass. Thus, this technique is not used to determine the $W$ mass. Instead, the muon momentum and electron energy scales are calibrated using the observed $Z$ mass peaks.

In the analysis of the 1988/1989 data, the Monte Carlo model uses MRS-B parton distribution functions (39). The transverse momentum distribution of the $W$ bosons is obtained from the observed $p_T^W$ distribution by an unfolding procedure. The results from the fits to the $m_T$ spectra in both decay channels are listed in Table 1. The combined result is $M_W = 79.91 \pm 0.39$ GeV.

In the analysis of the 1992/1993 data, parton distribution functions are restricted to those consistent with the measured charge asymmetry in $W \to \ell\overline{\nu}$ decays (23). The Monte Carlo model uses MRSD$-'$ (40). The transverse momentum distribution of the $W$ bosons is obtained from the observed $p_T^Z$ distribution, corrected

**TABLE 1** Comparison of individual $M_W$ measurement from $p\overline{p}$ colliders

| Measurement | | # Events | | $M_W$ | Errors (MeV) | | | |
|---|---|---|---|---|---|---|---|---|
| | | $W$ | $Z$ | (GeV) | Stat. | Scale | Syst. | Total |
| UA2 (6) | $e\overline{\nu}$ | 2065 | 251 | 80.36 | 220 | 260 | 150 | 370 |
| CDF (36) | $e\overline{\nu}$ | 1130 | N/A | 79.91 | 350 | 190 | 240 | 465 |
| | $\mu\overline{\nu}$ | 592 | N/A | 79.90 | 530 | 80 | 315 | 620 |
| CDF (22) | $e\overline{\nu}$ | 5718 | N/A | 80.49 | 145 | 120 | 130 | 230 |
| | $\mu\overline{\nu}$ | 3268 | N/A | 80.31 | 205 | 50 | 120 | 245 |
| DØ (42) | $e\overline{\nu}$ | 5982 | 366 | 80.35 | 140 | 160 | 145 | 255 |
| DØ (20) | $e\overline{\nu}$ | 23068 | 2179 | 80.44 | 70 | 70 | 60 | 115 |
| DØ (43) | $e\overline{\nu}$ | 11090 | 1687 | 80.69 | 110 | 190 | 75 | 230 |
| CDF (37) | $e\overline{\nu}$ | 30100 | 1600 | 80.47 | 65 | 75 | 55 | 115 |
| | $\mu\overline{\nu}$ | 14700 | 1800 | 80.47 | 100 | 85 | 55 | 145 |

for electron resolution and scaled so that the spectrum of the component of $\vec{u}_T$ perpendicular to the direction of the charged lepton agrees with the $W$ data. The underlying event model uses a lookup table of $\vec{u}_T$ versus generated $\vec{p}_T^{\,W}$, built from the $Z \to e^+e^-$ event sample. The results from the fits to the $m_T$ spectra in both decay channels are listed in Table 1. Their combined value is $M_W = 80.41 \pm 0.18$ GeV.

In the analysis of the 1994/1995 data, MRS-R2 (41) parton distribution functions are used. The $p_T^W$ spectrum is derived from the observed $p_T^Z$ spectrum, corrected based on a theoretical calculation of the ratio of the $p_T^W$ and $p_T^Z$ spectra (27, 28). The parameterized recoil model is tuned to $W$ and $Z$ data. The results from the fits to the $m_T$ spectra in both decay channels are listed in Table 1. Their combined value is $M_W = 80.470 \pm 0.089$ GeV.

All CDF measurements combined give $M_W = 80.433 \pm 0.079$ GeV.

### 2.2.3 DØ Experiment

The DØ collaboration has published three measurements of the $W$ boson mass using the $W \to e\overline{\nu}$ channel. Two measurements, using data from 1992/1993 (42) and 1994–1996 (20), use only electrons in the central calorimeter. The third measurement uses only data with the electron in the end calorimeters (43).

The DØ detector (8) uses a hermetic uranium–liquid argon sampling calorimeter, which encloses a nonmagnetic tracking system and is surrounded by a muon spectrometer.

The tracking system consists of three nested cylindrical subdetectors: a vertex drift chamber, a transition radiation detector, and a central drift chamber. These detector components cover the pseudorapidity region $|\eta| < 1$. Forward drift chambers on either side extend the tracking coverage to $|\eta| < 3$. The chambers provide measurements of direction and energy loss of charged particles.

The calorimeter is composed of three sections housed in three cryostats. The central calorimeter covers $|\eta| < 1$ and the two end calorimeters cover $1 < |\eta| < 4$. The electromagnetic section is 21 radiation lengths deep and segmented radially into four layers and laterally into towers covering $\Delta\phi \times \Delta\eta = 0.1 \times 0.1$. It measures the energy of electromagnetic showers with a resolution of $\sigma/E = 13.5\%/\sqrt{E \sin\theta/\text{GeV}}$ and the shower centroid position with a resolution of 2.5 mm in azimuthal direction. The hadron calorimeter is 7–9 nuclear interaction lengths deep and provides hermetic coverage free of projective cracks.

The event selection for $W$ decay events requires $p_T^e > 25$ GeV, $p_T^\nu > 25$ GeV, and $u_T < 15$ GeV. The $W$ boson $p_T$ and rapidity spectra are determined by a theoretical calculation (27), constrained by the observed $p_T^Z$ spectrum (25), for the 1992/93 data, and the MRST parton distribution functions functions (25) (for the 1992/1993 data) and the MRST parton distribution functions (44) (for the 1994–1996 data). The electron energy scale calibration is mainly based on the observed $Z$ peak. Signals from $J/\psi$ and $\pi^0$ decays extend the scale to lower energies. Electron resolution and the recoil model parameters are determined from the $Z$ data.

**TABLE 2** Summary of combined measurements of the $W$ boson mass at $p\overline{p}$ colliders

| Experiment | $M_W$ (GeV) | Uncertainty (MeV) | |
|---|---|---|---|
| | | Total | Correlated |
| UA2 | 80.363 | 371 | 85 |
| CDF | 80.433 | 79 | 25 |
| DØ | 80.482 | 91 | 9 |



Based on the fit to the $m_T$ spectrum from the 1992/1993 data, the DØ collaboration measures[5] $M_W = 80.35 \pm 0.21 \pm 0.15$ GeV. Based on the 1994–1996 data, the DØ collaboration measures the $W$ boson mass using the $m_T$, $p_T^e$, and $p_T^\nu$ spectra for electrons in the central calorimeter and end calorimeters. Using the complete $6 \times 6$ covariance matrix, these results are combined to $M_W = 80.498 \pm 0.095$ GeV with $\chi^2 = 5.1$ for five degrees of freedom. By increasing the acceptance for electrons to pseudorapidity between $-2.5$ and 2.5, the sensitivity to the rapidity spectrum of the $W$ bosons is reduced from 15 MeV to 7 MeV. This is reflected in the reduced uncertainty due to proton structure.

All DØ measurements combined give $M_W = 80.482 \pm 0.091$ GeV.

## 2.3 Combined Results from $p\overline{p}$ Collider Experiments

Table 1 lists the individual measurements in the sequence of their publication. The number of $W$ boson events given in the table reflects the number of events included in the fit to the transverse mass spectrum. The number of $Z$ events is given if the $Z$ data were used to calibrate the lepton scale.

Three principal contributions to the total error are listed: the statistical error, the uncertainty in the lepton momentum, and the remaining systematic uncertainty. All uncertainties are rounded to the nearest 5 MeV.

In combining the results from the three $p\overline{p}$ collider experiments, correlations must be accounted for. Since the Monte Carlo models used by the three experiments were tuned independently based on experimental data, the detector models are independent. Uncertainties due to higher-order corrections are dominated by independent experimental uncertainties. The constraints on the $W$ $p_T$ spectra are dominated by statistical fluctuations in the respective $Z$ data samples and are therefore uncorrelated as well. Thus, the only significant correlation originates from the common uncertainty in the structure of the proton. Table 2 summarizes the combined data.

The combined result is

$$M_W(p\overline{p}) = 80.452 \pm 0.060 \text{ GeV} \qquad 10.$$

with $\chi^2 = 0.23$.

[5]Updated uncertainties (20) relative to original publication.

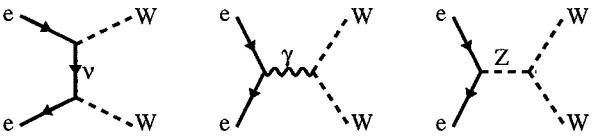


**Figure 7** The tree-level diagrams for the process $e^+e^- \rightarrow W^+W^-$: t-channel neutrino exchange and s-channel $\gamma$ and $Z^*$ exchange.



## 3. MEASUREMENTS OF $M_W$ AT LEP

From 1989 through 1995, LEP at CERN provided $e^+e^-$ collisions at center-of-mass energies at or near the $Z$ boson mass. Since 1996, LEP has been running at center-of-mass energies above the $W$ pair production threshold, $\sqrt{s} \geq 2\,M_W$. LEP delivers beams to four experiments, ALEPH, DELPHI, L3, and OPAL. While the LEP1 program afforded precision measurements of the $Z$ boson mass, the LEP2 program provides the opportunity to precisely measure the $W$ boson mass.[6]

At LEP2 energies, $W$ bosons are predominantly produced in pairs through the reaction $e^+e^- \rightarrow W^+W^-$, whose tree-level diagrams are shown in Figure 7. Each $W$ subsequently decays either hadronically ($q\overline{q}$) or leptonically ($\ell\overline{\nu}$, $\ell = e$, $\mu$, or $\tau$). There are three possible four-fermion final states, hadronic ($W^+W^- \rightarrow q\overline{q}q\overline{q}$), semileptonic ($W^+W^- \rightarrow q\overline{q}\ell\overline{\nu}$), and leptonic ($W^+W^- \rightarrow \ell\overline{\nu}\ell\overline{\nu}$), with branching fractions of 46%, 44%, and 10%, respectively. The $W^+W^-$ production cross section varies from 3.8 pb at $\sqrt{s} = 161$ GeV to 17.4 pb at $\sqrt{s} = 200$ GeV. This can be contrasted with the production cross sections for the dominant background processes,[7] $\sigma(e^+e^- \rightarrow Z/\gamma \rightarrow q\overline{q}) \sim 100-150$ pb, $\sigma(e^+e^- \rightarrow We\overline{\nu}) \sim 0.6$ pb, $\sigma(e^+e^- \rightarrow Z^0\,e^+e^-) \sim 2-3$ pb, and $\sigma(e^+e^- \rightarrow Z/\gamma Z/\gamma) \sim 0.5-1.5$ pb, where the spread accounts for variations over the range of LEP2 center-of-mass energies (45). The algorithms used to select candidate events exploit the kinematic properties unique to the $W^+W^-$ final states. The selection algorithms are sensitive to all possible $W^+W^-$ final states and obtain efficiencies of better than about 70% with purities in excess of about 80%.

### 3.1 Measurement Techniques

There are two main methods available to measure $M_W$ at LEP2. The first exploits the fact that the $W^+W^-$ production cross section is particularly sensitive to $M_W$ in the threshold region near $\sqrt{s} \approx 2M_W$. Assuming standard-model couplings and production mechanisms, a measure of the production cross section yields a

[6] "LEP1" refers to data taken from 1989 through 1995, when the LEP collider operated at about $\sqrt{s} = M_Z$; "LEP2" refers to data taken from 1996 through 2000 at $\sqrt{s} = 161 - 205$ GeV.

[7] Some of the cross sections given here include kinematic cuts that restrict the final-state phase-space. These cuts are detailed in Reference 45.

measure of $M_W$. In early 1996 each of the LEP experiments collected roughly 10 pb$^{-1}$ of data at $\sqrt{s} = 161$ GeV and determined $M_W$ using the threshold technique (46).

The second method uses the shape of the reconstructed invariant mass distribution to measure $M_W$. This method is particularly useful for $\sqrt{s} \geq 170$ GeV where the $W^+W^-$ production cross section is larger and phase-space effects on the reconstructed mass distribution are smaller. Each experiment collected roughly 10 pb$^{-1}$ at $\sqrt{s} = 172$ GeV (47) in late 1996, 55 pb$^{-1}$ at $\sqrt{s} = 183$ GeV in 1997 (48), 180 pb$^{-1}$ at $\sqrt{s} = 189$ GeV in 1998 (49), and 225 pb$^{-1}$ at $\sqrt{s} = 192 - 202$ GeV in 1999. Since most of the LEP2 data have been collected at center-of-mass energies well above the $W^+W^-$ threshold, the LEP2 $M_W$ determination is dominated by the direct reconstruction method. The results reported in this article are based on data taken through the end of 1998. Each method is described in greater detail below.

## 3.2 Threshold Determination of $M_W$

At center-of-mass energies very near 2 $M_W$, the $W^+W^-$ production cross section, $\sigma_{WW} \equiv \sigma(e^+e^- \rightarrow W^+W^-)$, is a strong function of $M_W$, so that a measurement of $\sigma_{WW}$ can be used to determine the $W$ boson mass. This is illustrated in Figure 8, which shows the $W$ pair production cross section as a function of center-of-mass energy for various assumed values of the $W$ boson mass. Note that for $\sqrt{s}$ significantly above or below 2 $M_W$, the various curves converge, so that $\sigma_{WW}$ has little sensitivity to $M_W$ at those energies. It is only in the threshold region that the

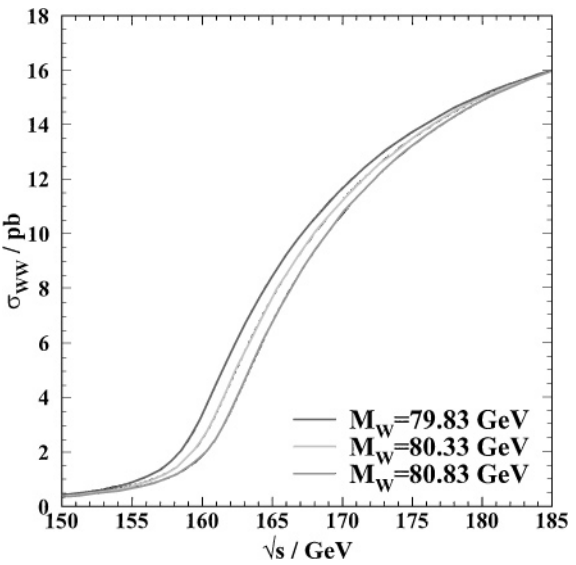


**Figure 8** The $e^+e^- \rightarrow W^+W^-$ cross section as a function of $\sqrt{s}$ for various $M_W$ values.

curves significantly separate, so that a measure of $\sigma_{WW}$ affords a determination of $M_W$. To measure the $W$ boson mass using the threshold method, it is necessary to (*a*) select events, (*b*) determine $\sigma_{WW}$, and (*c*) extract $M_W$ from the $\sigma_{WW}$ determination. In practice, steps (*b*) and (*c*) are not completely independent owing to quantum interference effects, which have to be taken into account in the definition of the $W^+W^-$ production cross section.

The $W$ pair production cross section is defined as the production cross section for the diagrams given in Figure 7. The separation between the signal $W^+W^-$ production diagrams and background diagrams resulting in the same four-fermion final states (e.g. $e^+e^- \rightarrow W^+W^- \rightarrow u\bar{d}\bar{u}d$ and $e^+e^- \rightarrow Z^*\,Z^* \rightarrow u\bar{u}d\bar{d}$) is complicated by quantum interference effects. In addition, the cross section $\sigma_{WW}$ is affected by higher-order electroweak and QCD corrections. The effects of four-fermion interference and the electroweak and QCD corrections must all be sufficiently understood theoretically in order to determine $M_W$. In practice, the interference effects are small and can be sufficiently addressed in the background subtraction, as discussed in Section 3.2.5. The effects of the higher-order corrections are larger and are discussed below.

As illustrated in Figure 9 (45), the $\sigma_{WW}$ cross section is impacted near $2\,M_W$ by the effects of the natural width of the $W$ boson, $\Gamma_W$, and by the effects of initial-state radiation (ISR). There are also large corrections associated with Coulomb interactions between the two $W$s, and some QCD corrections affecting $W^+W^- \rightarrow$

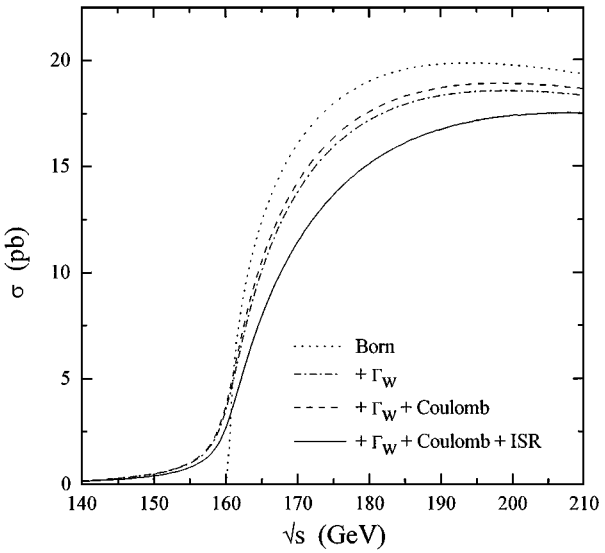


**Figure 9** The $e^+e^- \rightarrow W^+W^-$ cross section as function of $\sqrt{s}$ based on the on-shell (Born) approximation, plus including various corrections for the effect of the $W$ boson width ($\Gamma_W$), the Coulomb radiation between $W^+W^-$, and initial-state radiation (ISR) (45).

$q\overline{q}f\overline{f}$ final states. The theoretical uncertainties associated with these necessary corrections contribute a 2% uncertainty in $\sigma_{WW}$. These theoretical uncertainties are dominated by the uncertainty in the Higgs boson mass, which contributes to higher-order electroweak loop corrections and is most pronounced near threshold (1.5%). The remaining uncertainties contribute below the 0.5% level (50).

### 3.2.1 Event Selections

The statistical uncertainty in $M_W$ determined from the threshold method can be expressed as

$$\Delta M_W(\text{stat}) = \sqrt{\sigma_{WW}} \left| \frac{\mathrm{d}M_W}{\mathrm{d}\sigma_{WW}} \right| \frac{1}{\sqrt{\varepsilon_{\text{WW}} \mathcal{L} \mathcal{P}}}, \qquad 11.$$

where $\varepsilon_{\text{WW}}$ and $\mathcal{P}$ are the $W^+W^-$ selection efficiency and purity, respectively, and $\mathcal{L}$ is the total integrated luminosity. From this equation it is obvious that high-efficiency, high-purity selections are important. Separate selections are developed for each of the main four-fermion final states—the fully hadronic, the semileptonic, and the fully leptonic. Each is discussed separately below. The algorithms employed are quite involved and vary in the details of their implementation for the LEP experiments. We attempt here simply to emphasize the most important discriminating variables and the dominant systematic uncertainties. (See Reference 46 for detailed descriptions of the selection algorithms.)

### 3.2.2 $W^+W^- \rightarrow q\overline{q}q\overline{q}$ Event Selection

The fully hadronic selection is designed to efficiently select $W^+W^- \rightarrow q\overline{q}q\overline{q}$ events, which are characterized by four (or more) energetic hadronic jets, with little missing energy or momentum. The dominant background is from the QCD processes $e^+e^- \rightarrow \mathrm{Z}/\gamma \rightarrow q\overline{q}(+ng)$, which radiate little energy to ISR. Discrimination relies primarily on the fact that the jets in signal events tend to be higher-energy and have a more spherical distribution than those in background events. To further reduce the QCD background, a kinematic fit can be used that requires the two dijet masses to be approximately equal. The selections usually require high-multiplicity, full-energy events and exploit the unique $W^+W^- \rightarrow q\overline{q}q\overline{q}$ kinematics in a multivariate discriminant (e.g. a neural net output) to separate signal from background. The typical selection efficiency is about 55% with 80% purity.

For the background estimate, the dominant systematic uncertainty (5%) is associated with modeling the QCD background, which is estimated by comparing data to Monte Carlo distributions using high-statistics samples of $e^+e^- \rightarrow Z^0 \rightarrow q\overline{q}$ events from LEP1, and by comparing the estimates from different Monte Carlo generators, PYTHIA and HERWIG. The uncertainty associated with the signal efficiency is dominated by differences in the Monte Carlo generators (PYTHIA, HERWIG, ARIADNE, KORALW, and EXCALIBUR). Contributions from uncertainties in the LEP beam energy, $E_{\text{bm}}$, and ISR are negligible (<1%). The selection efficiency is also

negligibly dependent on $M_W$ and on the details of modeling color-reconnection (CR) and Bose-Einstein (BE) correlation effects, which are discussed in more detail in Section 3.3.4.

### 3.2.3 $W^+W^- \to q\bar{q}\ell\bar{\nu}$ Event Selection

The semileptonic selection is designed to efficiently select $W^+W^- \to q\bar{q}\ell\bar{\nu}$ events and is typically broken into three separate selections, one for each lepton flavor.

The $W^+W^- \to q\bar{q}e\bar{\nu}$ and $W^+W^- \to q\bar{q}\mu\bar{\nu}$ events are characterized by two energetic hadronic jets, a high-energy, isolated lepton, and a large missing momentum associated with the prompt neutrino. The dominant background is from radiative $e^+e^- \to Z/\gamma \to q\bar{q}$ events in which a hadron or initial-state photon is misidentified as a lepton. Other background sources are $e^+e^- \to We\bar{\nu}$, $e^+e^- \to ZZ$, and $e^+e^- \to Ze^+e^-$ events. The selections require two hadronic jets, an energetic (e.g. $E > 25$ GeV), isolated electron or muon, and large missing momentum. The backgrounds from radiative $e^+e^- \to q\bar{q}$ and $e^+e^- \to We\bar{\nu}$ events tend to produce missing momentum along the beam axis. Requiring a significant missing transverse momentum dramatically reduces these backgrounds. The typical selection efficiency is about 70–80% with purities of around 95%. These selections also select about 5% of $W^+W^- \to q\bar{q}\tau\bar{\nu}$ events because of the leptonic decays of the $\tau$ lepton.

The dominant systematic uncertainty associated with the selection efficiencies (2%) is due to uncertainties in the Monte Carlo modeling of the data and different Monte Carlo generators for $e^+e^- \to W^+W^-$ events. The dominant systematic uncertainty (30–50%) associated with the background estimate is due to the modeling of the dominant $e^+e^- \to Z/\gamma \to q\bar{q}$ background and from comparisons of different Monte Carlo generators. For the $W^+W^- \to q\bar{q}e\bar{\nu}$ channel, uncertainties from the modeling of four-fermion interference, particularly from $e^+e^- \to We\bar{\nu}$ events, estimated by comparing the results of different Monte Carlo generators, can increase the total background uncertainty to 100%. Because the selections are so pure, these relatively large uncertainties in the accepted background cross sections translate into very small uncertainties in $\sigma_{WW}$.

The $W^+W^- \to q\bar{q}\tau\bar{\nu}$ events are characterized by two hadronic jets, a $\tau$ decay jet, and missing momentum associated with two or more neutrinos. The dominant background arises from radiative $e^+e^- \to Z/\gamma \to q\bar{q}$ events in which a third jet, often due to soft gluon emission, is misidentified as a $\tau$ jet. These selections are very similar to the $W^+W^- \to q\bar{q}e\bar{\nu}$ and $W^+W^- \to q\bar{q}\mu\bar{\nu}$ selections except that they identify the $\tau$ as a low-mass, low-multiplicity (1- or 3-prong), isolated jet. Since the lepton identification is looser than for the other $W^+W^- \to q\bar{q}\ell\bar{\nu}$ selections, the background tends to be higher. Selection efficiencies vary widely among the LEP experiments—from 35% to 45% exclusive of those $W^+W^- \to q\bar{q}\tau\bar{\nu}$ events identified by one of the other selections. Because of the looser lepton identification requirements, these algorithms typically select an additional 3–5% of

$W^+W^- \to q\overline{q}e\overline{\nu}$ and $W^+W^- \to q\overline{q}\mu\overline{\nu}$ events that fail the above selections. The typical purity of this selection also varies widely among the LEP experiments, 65–85%.

The dominant systematic uncertainty associated with the selection efficiency (2.5%) is due to the modeling of the lepton identification variables, estimated by comparing LEP1 data and Monte Carlo, and the comparison of various Monte Carlo generators. The dominant systematic uncertainty associated with the estimate of the accepted background cross section (20%) comes from the modeling of hadron misidentification, estimated by comparing the data and Monte Carlo fake rates in LEP1 $e^+e^- \to Z^0 \to q\overline{q}$ events.



### 3.2.4 $W^+W^- \to \ell\overline{\nu}\ell\overline{\nu}$ Event Selection

The fully leptonic channel, $W^+W^- \to \ell\overline{\nu}\ell\overline{\nu}$, is characterized by two high-energy, isolated, acoplanar leptons. The selections typically start by requiring a low multiplicity and large missing transverse momentum. There are six distinct $\ell\ell'$ final states ($ee$, $e\mu$, $e\tau$, $\mu\mu$, $\mu\tau$, and $\tau\tau$), which have different dominant background sources. Potential background sources are two-photon, $e^+e^- \to We\overline{\nu}$, $e^+e^- \to Z^0e^+e^-$, and radiative $e^+e^- \to Z^0\gamma \to \ell^+\ell^-\gamma$ events. In general the $W^+W^- \to \ell\overline{\nu}\ell\overline{\nu}$ selection involves several independent and overlapping sets of cuts that employ various combinations of specific electron, muon, and $\tau$ lepton identification algorithms. Backgrounds are usually rejected by requiring large missing energy, large transverse momentum, and a large lepton-lepton acoplanarity. The efficiency varies widely across the LEP experiments, from about 45% for DELPHI and L3 to about 65% for OPAL and ALEPH. The selection purities are around 90–95%.

The dominant systematic uncertainty associated with estimating the selection efficiency (2%) is due to the modeling of lepton identification variables, specifically those sensitive to the modeling of final-state radiation (e.g. isolation variables). Uncertainties in the Monte Carlo generators also contribute. The dominant systematic uncertainty associated with estimating the accepted background cross sections (70%) arises from limited Monte Carlo statistics and comparisons of different Monte Carlo generators. The effect of detector modeling uncertainties is small owing to the experience gained at LEP1 using $e^+e^- \to Z^0 \to \ell^+\ell^-$ data. However, veto cuts employed in these low-multiplicity final states are particularly sensitive to beam-related backgrounds, which are not included in the Monte Carlo simulations. These are estimated using random trigger crossings and have the consequence of reducing both the signal efficiency and accepted background by a factor of 0.95–1.0 with a relative uncertainty of a few percent.

### 3.2.5 Determining $\sigma_{WW}$ and $M_W$

A maximum likelihood procedure is used to determine $\sigma_{WW}$. The likelihood is usually taken to be the product of Poisson probabilities of observing $N_i$ events when expecting $\mu_i(\sigma_{WW}) = \mathcal{L} \cdot [\sigma_{WW} \cdot \mathcal{B}_i \cdot \varepsilon_i + \sigma^{\text{acc}}_{\text{bgd}_i}]$ events, where $\varepsilon_i$, $\mathcal{B}_i$, and $\sigma^{\text{acc}}_{\text{bgd}_i}$ are the selection efficiency, branching ratio, and accepted background cross section, respectively, for the $i$th selection, and $\mathcal{L}$ is the integrated luminosity. In the

likelihood calculation, correlations between the channels are properly accounted for and standard-model branching ratios are assumed. The accepted background cross section is assumed to be independent of $M_W$. Four-fermion interference effects are typically accounted for either by applying a correction factor, $f_i$, to the product $\sigma_{WW}\mathcal{B}_i \to \sigma_{WW}\mathcal{B}_i f_i$, or by adding a term, $F_i$, to $\sigma_{\mathrm{bgd}_i}^{\mathrm{acc}} \to \sigma_{\mathrm{bgd}_i}^{\mathrm{acc}} + F_i$. These corrections are negligible ($|1 - f_i| < 1\%$) for all channels except the $q\bar{q}e\bar{\nu}$ and $\ell\bar{\nu}\ell\bar{\nu}$ channels, which have $f_{q\bar{q}e\bar{\nu}} \approx 1.09$ ($F_{q\bar{q}e\bar{\nu}} \approx -0.05$ pb) and $f_{\ell\bar{\nu}\ell\bar{\nu}} \approx 0.97$($F_{\ell\bar{\nu}\ell\bar{\nu}} \approx +0.01$ pb). These corrections factors are determined by comparing the predicted total accepted cross section (i.e. signal plus background) calculated including and excluding these interference effects. A systematic uncertainty is estimated by comparing the predictions from different Monte Carlo generators that include the four-fermion (4f) interference effects. Given the large statistical uncertainty on $\sigma_{WW}$, these corrections do not significantly affect the result. Strictly speaking, the correct manner in which to account for these interference effects is to make the replacement $\sigma_{WW} \to \sigma_{4\mathrm{f}}$ in the likelihood calculation, where $\sigma_{4\mathrm{f}}$ is the $M_W$-dependent four-fermion production cross section, including the interference effects.

The measured $W^+W^-$ production cross section is then compared to standard-model predictions for $\sigma_{WW}$ dependent on $M_W$ and $E_{\mathrm{bm}}$. The likelihood equation is modified so that $\sigma_{WW} \to \sigma_{WW}(M_W, E_{\mathrm{bm}})$. The dependence of $\sigma_{WW}$ on $M_W$ is calculated using the semi-analytic program GENTLE (51), which includes the higher-order electroweak and QCD corrections. The results from each of the LEP experiments are given in Table 3.

In addition to the systematic uncertainties associated with the selection efficiencies and accepted background cross sections described above, there are uncertainties due to higher-order corrections affecting $\sigma_{WW}(M_W, E_{\mathrm{bm}})$ (2% at $\sqrt{s} = 161$ GeV, as discussed above) and to the precision of the LEP determination of $E_{\mathrm{bm}}$ ($\pm 27$ MeV at $\sqrt{s} = 161$ GeV (52)).

### 3.2.6 Combined Determinations of $M_W$ from Threshold Data

The combined determination of $M_W$ is extracted from the LEP combined measurement of $\sigma_{WW}$, which is then compared to the GENTLE prediction for $\sigma_{WW}(M_W, E_{\mathrm{bm}})$ assuming standard-model couplings and the LEP average center-of-mass energy, as shown in Figure 10. When making the combination, the individual results are

**TABLE 3** Measurement of the *w* pair production cross section, $\sigma_{WW}$, and *W* boson mass, $M_W$, at $\sqrt{s} = 161$ GeV at LEP

| **Experiment** | $\sigma_{WW} \pm$ **(sta)** $\pm$ **(sys) (pb)** | $M_W \pm$ **(sta)** $\pm$ **(sys) (GeV)** | $\mathcal{L}$ **(pb$^{-1}$)** |
|---|---|---|---|
| ALEPH | $4.23 \pm 0.73 \pm 0.19$ | $80.14 \pm 0.34 \pm 0.09$ | 11 |
| DELPHI | $3.67^{+0.97}_{-0.85} \pm 0.19$ | $80.40 \pm 0.44 \pm 0.09$ | 10 |
| L3 | $2.89^{+0.81}_{-0.70} \pm 0.14$ | $80.80^{+0.47+0.09}_{-0.41-0.08}$ | 11 |
| OPAL | $3.62^{+0.93}_{-0.82} \pm 0.16$ | $80.40^{+0.44}_{-0.41} \pm 0.10$ | 10 |

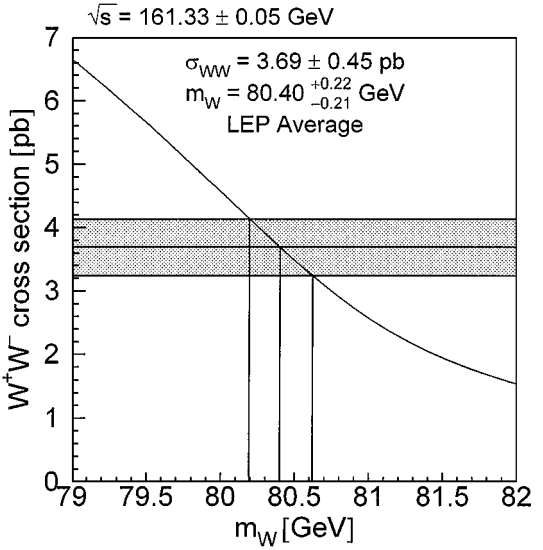


**Figure 10** The combined measurement of $\sigma_{WW}$ (shaded band) near threshold at LEP is compared to a semi-analytic calculation of $\sigma_{WW}$ ($M_W$, $\sqrt{s}$) using the LEP average center-of-mass energy to extract a value $M_W$ (53).



weighted by the expected statistical uncertainty so as to avoid biasing the results. Since the statistical uncertainties dominate each individual measurement as well as the combined result, the smallest quoted systematic uncertainty (0.14 pb) is conservatively taken to be fully correlated between experiments. Note that since an individual experiment's weight in the combination is driven by its statistical uncertainty, this procedure does not affect the central value of the combined result and yields a conservative estimate of the combined systematic uncertainty. Combining the four LEP results for $\sigma_{WW}$ yields

$$\sigma_{WW} = 3.69 \pm 0.45\,\text{pb} \qquad 12.$$

with a $\chi^2$ per degree of freedom of 1.3/3. Using the LEP average center-of-mass energy of 161.33 $\pm$ 0.05 GeV and the GENTLE prediction (51), the $W$ boson mass is then determined from this threshold (TH) method to be (53)

$$M_W(\text{TH}) = 80.400 \pm 0.220(\text{exp}) \pm 0.025(E_{\text{bm}})\,\text{GeV}. \qquad 13.$$

The statistical uncertainty dominates the experimental uncertainty, which has a contribution of approximately 70 MeV from correlated systematics. If this method were to be employed in the future, a potentially limiting uncertainty would arise from the modeling of fragmentation and hadronization, which has a large effect on the $W^+W^- \to q\bar{q}q\bar{q}$ channel and is correlated among the experiments. This uncertainty is presently the single largest contribution to the total uncertainty assigned to the LEP combined $\sigma_{WW}$ at higher center-of-mass energies (where the statistical uncertainties are smaller) and contributes an uncertainty of approximately 50 MeV to $M_W$(TH).

## 3.3 Direct Reconstruction of $M_W$

As demonstrated in Figure 8, at center-of-mass energies above 170 GeV the $W^+W^-$ production cross section becomes significantly less sensitive to $M_W$. At these energies, one can extract a measurement of $M_W$ from the invariant mass distribution of the $W$ decay products. The sensitivity to uncertainties associated with the modeling of events near the phase-space limit ($M_{W^+} = M_{W^-} = E_{\rm bm}$) is greatly reduced since $(\sqrt{s} - 2M_W) \gg \Gamma_W$. However, as discussed in Section 3.3.4, the modeling of various final state interactions becomes more important in the $W^+W^- \to q\overline{q}q\overline{q}$ channel. To measure $M_W$ using this direct reconstruction technique, it is necessary to (*a*) select events, (*b*) obtain the reconstructed invariant mass, $m_{\rm rec}$, for each event, and (*c*) extract a measurement of $M_W$ from the $m_{\rm rec}$ distribution. Each of these steps is discussed in detail in the sections below.

### 3.3.1 Event Selection

The expected statistical uncertainty on $M_W$ determined from direct reconstruction will vary inversely with the selection efficiency and purity. At higher center-of-mass energies, the $W^+W^-$ production cross section increases by more than a factor of four, whereas the dominant background cross sections increase less rapidly or even decrease. This affords selections with greater efficiencies for the same purities relative to those employed for the selection at $\sqrt{s} = 161$ GeV. Nevertheless, the algorithms employed are very similar to those described in Section 3.2.1 and so are not further discussed here. Typical selection efficiencies (purities) are 85% (80%) for the $W^+W^- \to q\overline{q}q\overline{q}$ channel, 90% (95%) for the $W^+W^- \to q\overline{q}e\overline{\nu}$ and $W^+W^- \to q\overline{q}\mu\overline{\nu}$ channels, and 65% (85%) for the $W^+W^- \to q\overline{q}\tau\overline{\nu}$ channel. The $W^+W^- \to \ell\overline{\nu}\ell\overline{\nu}$ channel does not significantly contribute to the determination of $M_W$ from direct reconstruction and is not discussed further. For the high-energy data taken through 1999, these efficiencies and purities yield approximately 7000 $W^+W^- \to q\overline{q}f\overline{f}$ candidate events, about 1100 of which are non-$W^+W^-$ background. The selection efficiencies have a total uncertainty of about 1% (absolute) and have a negligible effect (<1 MeV) on the $M_W$ determination. The accepted background cross sections have a total uncertainty of 10–20% (relative) and affect the $M_W$ determination at the level of 10–15 MeV (see Section 3.3.4).

### 3.3.2 Invariant Mass Reconstruction

For each selected event, an invariant mass is reconstructed from the $W$ decay products. There are several methods available for reconstructing the invariant mass of a $W$ candidate. The best resolution is obtained by using a kinematic fit which exploits the fact that the center-of-mass energy of the collision is known a priori.[8] Since the type of fit employed varies for each final state, we discuss each

[8]Strictly speaking, this is not true since any ISR reduces the collision energy to less than twice the beam energy. The kinematic fits assume no ISR. The effect of ISR uncertainties is incorporated in the total systematic uncertainty discussed in Section 3.3.4 and is small.

type separately. Although the details of the fits differ among the LEP experiments, the important features are similar.

Selected $W^+W^- \rightarrow q\overline{q}q\overline{q}$ events are forced into a four-jet configuration using, for example, the Durham algorithm (54). A kinematic fit is then performed to estimate the reconstructed invariant mass of the $W$ candidates. A fit that incorporates the constraints of energy and momentum conservation (4C fit) yields two reconstructed invariant masses per event ($m_{\mathrm{rec}_1}$, $m_{\mathrm{rec}_2}$), one for each $W$ boson in the final state. A fifth constraint can be incorporated by neglecting the finite $W$ width and constraining the two invariant masses to be equal, $m_{\mathrm{rec}_1} = m_{\mathrm{rec}_2}$. For each event, this 5C fit yields a single reconstructed mass, $m_{\mathrm{rec}}$, its uncertainty, $\sigma_{\mathrm{rec}}$, and a $\chi^2$ probability. The fit requires as input the jet momenta, energy, and their associated uncertainties. A complication of the $q\overline{q}q\overline{q}$ final state is due to the pairing ambiguity—there exist three possible jet-jet pairings for a four-jet final state. This pairing ambiguity gives rise to a combinatoric background unique to this channel. The LEP experiments employ various techniques to differentiate among the combinations. Typically an experiment uses the best one or two combinations. The correct combination is among those used in about 85–90% of the events. For events with the correct pairing, the kinematic fit has a resolution of about 0.7 GeV per event and is dominated by the jet angular resolution. The wrong combinations are treated as background. It should be noted that the shape of the combinatoric background is fairly flat (see Figure 11). As a result, the $M_W$ determination is not critically dependent on the fraction of correct pairings.

Selected $q\overline{q}e\overline{\nu}$ and $q\overline{q}\mu\overline{\nu}$ events are forced, after removing the lepton candidate, into a two-jet configuration. All four LEP experiments use a kinematic fit employing energy and momentum conservation constraints and the equal mass constraint. Since the prompt neutrino from the leptonically decaying $W$ removes three degrees of freedom, this is a 2C fit yielding a single reconstructed mass, uncertainty, and $\chi^2$ probability per event. The fit requires as input the jet and lepton energy and momenta and their associated uncertainties. The $q\overline{q}e\overline{\nu}$ and $q\overline{q}\mu\overline{\nu}$ events have a mass resolution of roughly 1.0 GeV and 1.1 GeV, respectively, per event. This resolution is dominated by the uncertainty in the lepton energy.

Selected $q\overline{q}\tau\overline{\nu}$ events are forced, after removing tracks and clusters associated with the $\tau$ decay, into a two-jet configuration. The treatment of $q\overline{q}\tau\overline{\nu}$ events varies among the LEP experiments, but all make use of the invariant mass of the hadronic system, the resolution of which can be improved by requiring energy and momentum conservation and employing the equal mass constraint. The mass resolution for the $q\overline{q}\tau\overline{\nu}$ events is approximately 1.5 GeV per event and is dominated by the resolution of the jet energies.

### 3.3.3 Extracting $M_W$

The ensemble of selected events yields a $m_{\mathrm{rec}}$ distribution from which a measure of $M_W$ is extracted. There are several methods available for extracting $M_W$. ALEPH, L3, and OPAL all use a traditional maximum likelihood comparison of

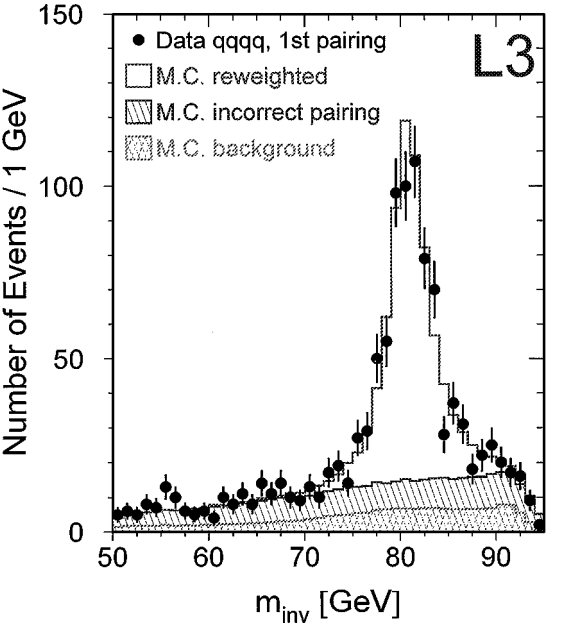


**Figure 11** Analysis of data from the L3 experiment for the $W^+W^- \to q\overline{q}q\overline{q}$ channel for data taken at $\sqrt{s} = 189$ GeV.

data to Monte Carlo spectra corresponding to different values of $M_W$. In addition to its simplicity, this method has the advantage that all biases (from resolution, ISR, selection, etc) are implicitly included in the Monte Carlo distributions. The disadvantage of this method is that it may not make optimal use of all available information. DELPHI employs a convolution technique, which makes use of additional information; in particular, events are weighted by the errors of the fit. The convolution is limited in that it requires various approximations (e.g. the resolution is often assumed to be Gaussian) and often requires an a posteriori correction because the fit procedure does not account for all biases, notably from ISR and selection. As a cross check of the fitting procedure, all experiments fit the data to a relativistic Breit-Wigner (with $s$-dependent width) plus background, which also requires a posteriori corrections. Since the dominant systematic uncertainties differ, $M_W$ is measured separately for the $q\overline{q}q\overline{q}$ and the $q\overline{q}\ell\overline{\nu}$ samples. The results are then combined, taking correlations into account, to yield an improved measurement of $M_W$. In the results given here, the standard-model relation between $M_W$ and $\Gamma_W$ has been assumed (50).

Table 4 displays the results from each LEP experiment, using data collected at $\sqrt{s} = 172$–$189$ GeV (47–49), for the $q\overline{q}\ell\overline{\nu}$ channel. Table 5 gives the results for the $q\overline{q}q\overline{q}$ channel.[9] Also included is the combined result of all the measurements.

[9]These results are based in part on preliminary numbers for the data taken at $\sqrt{s} = 189$ GeV.

**TABLE 4** LEP results for the $q\overline{q}\ell\overline{\nu}$ channel for data taken at $\sqrt{s} = 172$–$189$ GeV

| Experiment | $M_W \pm$ (stat) $\pm$ (syst)/(GeV) |
|---|---|
| ALEPH | $80.343 \pm 0.089 \pm 0.040$ |
| DELPHI | $80.297 \pm 0.141 \pm 0.064$ |
| L3 | $80.224 \pm 0.117 \pm 0.067$ |
| OPAL | $80.362 \pm 0.090 \pm 0.053$ |
| LEP | $80.313 \pm 0.052 \pm 0.036$ |



In the combination, correlations are taken into account, as described in Section 3.3.5. Figure 12 shows the OPAL fits for the data taken at $\sqrt{s} = 189$ GeV.

### 3.3.4 Systematic Uncertainties

Table 6 shows the systematic uncertainties for a "typical" LEP experiment. This table should be taken as a general guide. The actual numbers vary by as much as $\pm 20$ MeV from experiment to experiment. It is still the case that the total uncertainty of a single experiment is dominated by the statistical uncertainty. The experiments are at various stages in developing more sophisticated methods to estimate the limiting systematic uncertainties. This variation, and not any inherent detector or methodological advantage, largely accounts for the range of uncertainties.

For all four LEP experiments, the uncertainties associated with ISR, fragmentation, and four-fermion interference are limited by the statistics of the Monte Carlo samples used to estimate them. In Table 6, uncertainties associated with the selection efficiencies and accepted backgrounds are included in the row labeled "fit procedure." For the $q\overline{q}\ell\overline{\nu}$ channel, the largest single contribution to the systematic uncertainty is due to detector effects (e.g. energy scales, resolutions, and modeling). These uncertainties are expected to decrease as more data are

**TABLE 5** LEP measurements of $M_W$ for the $q\overline{q}q\overline{q}$ channel for data at $\sqrt{s} = 172$–$189$ GeV

| Experiment | $M_W \pm$ (stat) $\pm$ (syst) $\pm$ (CR/BE)/(GeV) |
|---|---|
| ALEPH | $80.561 \pm 0.095 \pm 0.050 \pm 0.056$ |
| DELPHI | $80.367 \pm 0.094 \pm 0.037 \pm 0.054$ |
| L3 | $80.656 \pm 0.104 \pm 0.071 \pm 0.092$ |
| OPAL | $80.345 \pm 0.098 \pm 0.074 \pm 0.055$ |
| LEP | $80.429 \pm 0.049 \pm 0.046 \pm 0.058$ |

**TABLE 6** Systematic uncertainties on $M_W$ from direct reconstruction for a "typical" LEP experiment

| | Uncertainty (MeV) | |
|---|---|---|
| **Systematic** | $q\bar{q}\ell\bar{\nu}$ | $q\bar{q}q\bar{q}$ |
| Initial-state radiation | 10 | 10 |
| Four-fermion | 10 | 10 |
| Fragmentation | 25 | 30 |
| Detector effects | 30 | 30 |
| Fit procedure | 20 | 20 |
| Subtotal | 46 | 49 |
| Beam energy | 17 | 17 |
| CR/BE | — | 60 |
| Total | 49 | 79 |

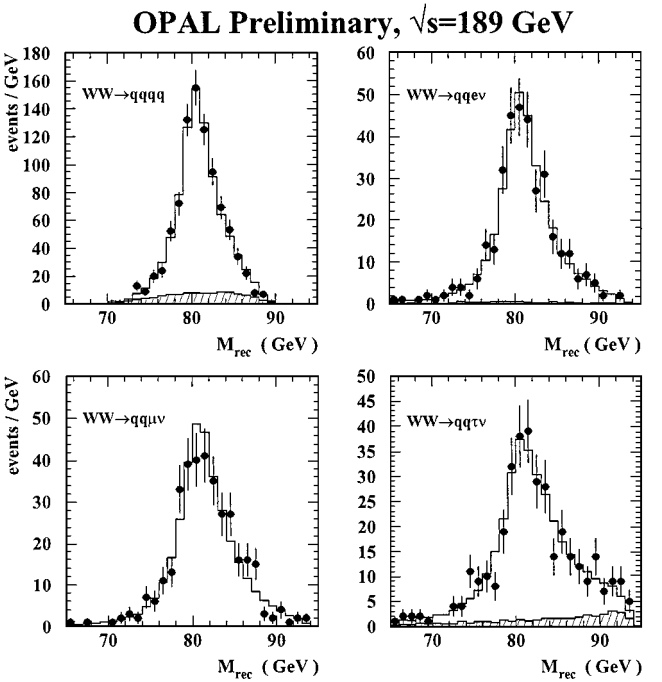


**Figure 12** Analysis of data from the OPAL experiment for data collected at $\sqrt{s} = 189$ GeV. The points are the data and the open histogram is the fit result. The non-*WW* background contribution, as estimated from Monte Carlo, is shown as a hatched histogram.

collected. For the $q\overline{q}q\overline{q}$ channel, the dominant systematic uncertainty is due to color-reconnection (CR) and Bose-Einstein (BE) correlation effects. Each source of uncertainty and the methods for estimating it are briefly described below.

***Initial-State Radiation*** Uncertainties due to the modeling of ISR are estimated by comparing the $m_{\rm rec}$ distributions of Monte Carlo samples, which include ISR corrections to differing orders. The standard Monte Carlo simulations include corrections to next-to-leading-log $\mathcal{O}(\alpha^2)$. The differences are negligible in samples of several million events. The uncertainty is conservatively taken to be 10 MeV.

***Four-Fermion Interference*** The systematic uncertainty associated with the modeling of four-fermion interference effects is usually estimated by comparing fit results for matrix element calculations including and excluding the interferences. The differences are small and the comparisons often statistically limited.

***Fragmentation*** A variety of methods are employed to estimate the uncertainty associated with fragmentation modeling. Typically, LEP1 data are used to constrain model parameters. Those parameters are then varied in several Monte Carlo samples, which are refit as data. The results are compared to that obtained with the default parameters. The differences are typically small except for the $W^+W^- \rightarrow q\overline{q}q\overline{q}$ channel, where they are on the order of 30 MeV. Because this systematic is strongly correlated among LEP experiments, it is one of the dominant systematic uncertainties in the LEP combined measurement. DELPHI employs an alternative method for estimating these uncertainties (48), in which two $Z^0 \rightarrow q\overline{q}$ events are boosted to the appropriate center-of-mass energy and overlayed for data and Monte Carlo and the resulting fit masses are compared.

***Detector Effects*** Calibration data collected at the start and end of each year at $\sqrt{s} = M_Z$ are used to establish limits on the uncertainties associated with detector modeling in the Monte Carlo. Uncertainties in energy scale and resolution are estimated using $Z^0 \rightarrow e^+e^-, \mu^+\mu^-, q\overline{q}$ data. The linearity is checked using Bhabha, $e^+e^-\gamma$, and three-jet events in data collected at higher center-of-mass energies. The angular resolutions are similarly determined. Typically the jet and lepton energy scales are known to within 0.5%, whereas the modeling of the angular and energy resolutions has associated uncertainties of the order of 5–20% depending on polar angle. These uncertainties are propagated to the $M_W$ measurement by comparing the fit results of Monte Carlo samples in which the appropriate quantity has been scaled or varied to the results from the default Monte Carlo sample. The observed differences are used as estimates of the associated uncertainty on $M_W$ due to detector modeling effects.

***Fit Procedure*** The type of effects considered depends on the fit method used to extract $M_W$ from the $m_{\rm rec}$ distribution. These include uncertainties associated

with the background normalization and shape, and fit biases. In general the total effect is very similar across methods. The background normalization is varied within uncertainties determined from a dedicated $\sigma_{WW}$ analysis and yields small effects. The shape of the background $m_{\rm rec}$ distribution is checked using data where possible and compared across different Monte Carlo generators otherwise, also yielding small effects. The linearity of the fit methods is determined from Monte Carlo samples generated assuming various $M_W$ values. These samples are also used to verify that the statistical uncertainty is accurate. For the convolution and Breit-Wigner methods, these Monte Carlo samples are used to calculate the necessary bias corrections, whose uncertainties are then propagated to the final uncertainty.

***Beam Energy*** The uncertainty in the beam energy enters via the constraints imposed by the kinematic fit and should be of the order of $dM_W = M_W \frac{dE_{bm}}{E_{bm}}$. The effect on the measured $M_W$ is estimated by refitting all data, changing the value of $E_{\rm bm}$ used in the fit, and calculating the mean difference in fitted $m_{\rm rec}$ on an event-by-event basis. The beam energy is estimated using the method of resonant depolarization (55), which has been performed up to $E_{\rm bm} \approx 60$ GeV. An extrapolation is required to estimate the beam energies at which the data are taken, $E_{\rm bm} \approx 100$ GeV, which results in an uncertainty in the beam energy of about 20 MeV. With the addition of more resonant depolarization data and new techniques, it is expected that the uncertainty on $M_W$ due to uncertainties in $E_{\rm bm}$ will be reduced to 10 MeV (52, 56). The spread in the beam energy, $\sigma_{E_{\rm bm}} \approx 150$ MeV (52), has a negligible effect on $M_W$.

***Color Reconnection/Bose-Einstein*** Since the typical decay distance of the $W$ bosons, $1/\Gamma_W \approx 0.1$ fm, is much smaller than the typical fragmentation radius, $1/\lambda_{QCD} \approx 1$ fm, the decay products originating from *different* $W$ bosons cannot be considered independent—i.e. they can "talk" to each other. The modeling of this cross-talk in the Monte Carlo spectra used to extract $M_W$ is an additional source of systematic uncertainty in the $W^+W^- \to q\overline{q}q\overline{q}$ channel. The cross-talk can arise through two mechanisms, BE correlations and CR effects (45, 57). The modeling uncertainty is estimated separately for BE and CR and is model-dependent in both cases. In each case, Monte Carlo samples employing implementations of various CR/BE models are treated as data and an $M_W$ bias is estimated. The systematic uncertainty is chosen to include the full range of variation among the models explored and is of the order of 50–60 MeV.

There has been recent progress in experimentally constraining the available CR models by comparing event shape and charged particle multiplicity distributions as predicted by various Monte Carlo models (both including and excluding CR effects) with those observed in the high-energy data. In addition, studies using LEP1 data can be used to test the available models (58). On the basis of these studies, some of the models have been excluded because they do not adequately describe the data (59), thus enabling a reduction in the associated systematic uncertainty (from ≈100 to ≈50 MeV). (See Reference 59 for a more complete

discussion.) Additional data should help to further constrain the remaining CR models and thus further reduce this uncertainty.

### 3.3.5 Combination of $M_W$ Determinations from Direct Reconstruction

Each of the LEP experiments provides a measured $W$ Boson mass for the fully hadronic and semileptonic channels separately for each center-of-mass energy, along with a matrix of associated uncertainties. The uncertainties are broken down into four components:

1. uncertainties uncorrelated between channels and experiments (e.g. the statistical uncertainty or background normalization and shape uncertainties);
2. uncertainties correlated among the channels of a given experiment but uncorrelated between experiments (e.g. detector modeling uncertainties);
3. uncertainties uncorrelated between the channels but correlated among the experiments (i.e. CR/BE uncertainties);
4. uncertainties correlated between the channels and among the experiments (e.g. ISR, fragmentation, $E_{\rm bm}$ uncertainties).

In this way, the correlations between channels and among experiments are accounted for. The correlation of the $E_{\rm bm}$ uncertainty across the different years is also taken into account. The results for the combined $q\overline{q}q\overline{q}$ and $q\overline{q}\ell\overline{\nu}$ channels are given in the last lines of Tables 4 and 5 and are 25% correlated with a $\chi^2/dof = 17.9/20$. Combining all the direct reconstruction (DR) results into a single mass yields

$$M_W(\mathrm{DR}) = 80.347 \pm 0.036\ (\mathrm{stat}) \pm 0.036\ (\mathrm{syst}) \pm 0.020\ (\mathrm{CR/BE}) \pm 0.017\ (E_{\rm bm})\ \mathrm{GeV},$$

where the uncertainties associated with CR/BE modeling and with the LEP beam energy are listed separately (60). The dominant systematic uncertainty is associated with the fragmentation model, which is correlated among the experiments (they all employ the same models in their Monte Carrlo simulation) and contributes an uncertainty of approximately 20 MeV. The effect of the CR/BE uncertainty is to de-weight the $q\overline{q}q\overline{q}$ measurements relative to the measurements in the $q\overline{q}\ell\overline{\nu}$ channels.

## 3.4 Combination of LEP Results

The $M_W$ determination from the threshold method is combined with the determination from the direct reconstruction method, taking account of the correlations. In particular, the systematic uncertainties associated with the LEP beam energy, and the modeling of ISR, fragmentation, and four-fermion interference effects are taken as correlated. Note that the weight of the threshold determination of $M_W$ in

the combination is driven by the statistical uncertainty of that measurement. The LEP combined result, assuming the standard-model relation between the *W* decay width and mass, is

$$M_W(\text{LEP}) = 80.350 \pm 0.056\ \text{GeV}, \qquad 14.$$

where the uncertainty includes both statistical and systematic uncertainties and is dominated by the determinations using direct reconstruction methods (60).



## 4. WHAT DO THESE MEASUREMENTS TELL US?

### 4.1 Combination of Results

Direct measurements of the *W* boson mass have been performed in two kinds of experiments, the production of *W* bosons in $p\overline{p}$ collisions and the production of $W^+W^-$ pairs in $e^+e^-$ collisions.

Until 1996, $p\overline{p}$ collisions were the only source of *W* bosons. The advantage of $p\overline{p}$ colliders lies in the large *W* production cross section and the low background levels. The $p\overline{p}$ data give about 100,000 $W \to \ell\overline{\nu}$ candidate events with about 97% purity. The production of *Z* bosons, dynamically and kinematically very similar to *W* boson production, provides a very convenient control data sample. The disadvantage of $p\overline{p}$ colliders is that the parton center-of-mass frame is not known on an event-by-event basis and therefore systematic effects arising from the structure of the protons must be understood. The combined $p\overline{p}$ collider measurement is $M_W$ $(p\overline{p}) = 80.452 \pm 0.060$ GeV.

Since 1996, $e^+e^-$ collisions with enough energy to produce pairs of *W* bosons have become available. The advantage of $e^+e^-$ collisions is that the initial particles are pointlike, and so the center-of-mass energy of the collision is known. Thus, kinematic fits can be employed to fully reconstruct events and yield invariant mass resolutions comparable to the *W* boson width. The disadvantage of $e^+e^-$ colliders is that the $W^+W^-$ production cross section is two orders of magnitude smaller than at $p\overline{p}$ colliders, resulting in smaller and less pure event samples (about 22,000 events with about 90% purity). In addition, the modeling of final-state interactions in $W^+W^- \to q\overline{q}q\overline{q}$ events must be understood. The combined LEP measurement is $M_W(\text{LEP}) = 80.350 \pm 0.056$ GeV. The two determinations of the *W* boson mass are completely uncorrelated. A combination of both results is simple, resulting in a world average of

$$M_W = 80.398 \pm 0.041\ \text{GeV} \qquad 15.$$

with a $\chi^2$ of 1.6. Having two independent, precise determinations of this parameter in agreement with each other lends significant credibility to the results.

Within the framework of the standard model, the measurement of the *W* boson mass determines the radiative corrections, $\Delta r$, in Equation 6. These corrections

have a large contribution from the running of the electromagnetic coupling. We can absorb this into the value of $\alpha$ by writing

$$\frac{\alpha}{1-\Delta r} = \frac{\alpha\left(M_Z^2\right)}{1-\Delta r_{\rm ew}}. \qquad 16.$$

For the residual contribution from electroweak loop diagrams, we find $\Delta r_{\rm ew} = -0.0268 \pm 0.0027$, about 10 standard deviations from zero.

## 4.2 Comparisons and Constraints Within the Standard Model

The standard model provides a framework that allows us to relate the measurements from many processes that involve the electroweak interaction. The main sources of such information are measurements of the properties of the $Z$ boson at LEP1 and the Stanford Linear Collider (SLC), the study of deep inelastic neutrino scattering at Fermilab, and the measurement of the mass of the top quark at the Tevatron.

LEP1 and SLC have provided a wealth of very precise measurements of the properties of the $Z$ boson (61). At tree level, the properties of the $Z$ boson are determined by its mass, the weak mixing angle, and the fine structure constant. Radiative corrections are dominated by the masses of the top quark and the Higgs boson. The wonderful success of the standard model lies in all measurements being consistent with single values of these parameters. The mass of the $Z$ boson is measured directly from the line shape, and the fine structure constant, evolved to $Q^2 = M_Z^2$, is derived from measurements of $R$, which is the ratio of the $e^+e^-$ cross sections to hadrons and to $\mu^+\mu^-$. The other three parameters are extracted from a fit to the measurements. The $W$ mass then follows from Equation 6.

The CCFR (62) and NuTeV (63) experiments at Fermilab measure the ratio of charged-current and neutral-current interactions of neutrinos. This ratio depends directly on $1 - M_W^2/M_Z^2$. From the measured value $1-M_W^2/M_Z^2 = 0.2255 \pm 0.0021$,[10] a value for the $W$ boson mass of $M_W = 80.250 \pm 0.109$ GeV can be derived.

At the loop level, many other parameters contribute (mostly negligible) corrections to the tree-level values. Due to the large mass difference between the top and bottom quarks, radiative corrections involving top quark loops are important. The CDF and DØ collaborations have measured the top quark mass directly (64). Their combined value is $m_{top} = 174.3 \pm 5.1$ GeV.

A fit of the standard model to all measurements except the direct measurements of the $W$ boson mass returns (65) $M_W = 80.381 \pm 0.026$ GeV as its preferred value. This value is in excellent agreement with the combined direct measurements, in support of the validity of the standard model. The mass of the Higgs boson is the only parameter that has not been measured experimentally. Loops

[10] CCFR and NuTeV combined.

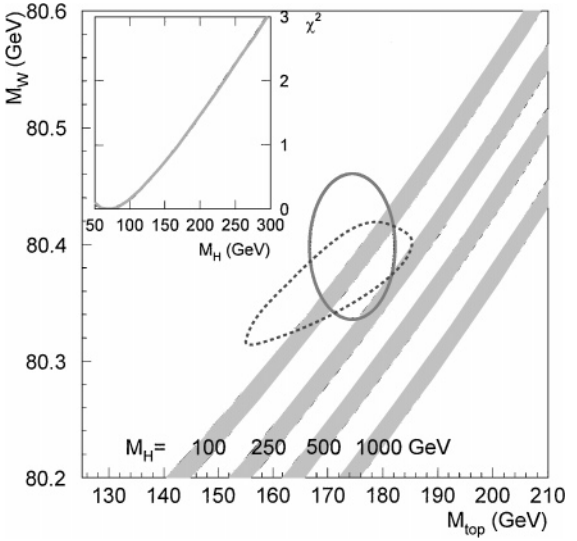


**Figure 13** Comparison of direct measurement of the *W* boson and top quark masses with indirect measurements (65) and predictions of the standard model (66). The indirect constraint is in part based on preliminary data.



containing Higgs bosons also contribute important radiative corrections. A fit to all electroweak data, including the measurements of the *W* boson mass, prefers $M_H = 77^{+69}_{-39}$ GeV for the mass of the Higgs boson (65).

The Higgs boson mass can also be constrained based on the measured values of the *W* boson and top quark masses alone. This is shown graphically in Figure 13. The shaded bands indicate the values of the *W* boson mass predicted by the standard model as a function of the top quark mass, for given values of the Higgs boson mass (66). The width of the bands indicates the variation due to the uncertainty in $\alpha(M_{Z^2})$ (67), which dominates the uncertainty in the predictions. The ellipse indicates the two-dimensional 68% confidence-level interval defined by the measured mass values. The inset shows a plot of $\chi^2$ between the measured values and the predictions as a function of the Higgs boson mass. The preferred Higgs boson mass is $71^{+96}_{-51}$ GeV. Values above 277 GeV are excluded at 90% confidence level. The dashed contour shows the 68% confidence-level interval from the fit to all other electroweak data (65).

## 4.3 Constraints Outside the Standard Model

Any particle that couples to the *W* boson can contribute loop corrections to the value of the *W* boson mass. Thus a measurement of the *W* boson mass not only tests the standard model but is also, at least in principle, sensitive to nonstandard physics. In the minimal supersymmetric model, corrections could increase the *W* boson mass by as much as 250 MeV (68). The lower the scale of supersymmetry breaking, the larger the correction. If the scale of supersymmetry breaking is more than a few hundred GeV, supersymmetry decouples from standard-model

physics and the effects of supersymmetric loop corrections on the $W$ boson mass become small. Supersymmetric particles that give large corrections must be relatively light and would also be the first ones to be seen in direct searches. Thus, precision measurements are unlikely to increase the sensitivity of direct searches for supersymmetric extensions of the standard model.

## 5. FUTURE PROSPECTS



The precision on the world average $W$ mass measurement is expected to improve significantly over the next five years, and more dramatically over the next decade or so.

By the end of 2000, the LEP experiments will have more than doubled the statistics of their $W^+W^-$ data sets relative to those discussed here. The inclusion of the additional data will yield a statistical uncertainty of about 25 MeV for the combined LEP measurement of $M_W$. Already a significant effort has been made to reduce the systematic uncertainties, particularly those associated with the detector energy scales and resolutions. It is expected that these errors can be brought to the 20 MeV level. The additional constraints afforded by the LEP spectrometer project (56) and by additional depolarization data make it likely that the uncertainty associated with the LEP beam energy will be reduced to roughly 10 MeV. It is difficult to predict how the systematic uncertainties associated with the modeling of BE and CR effects in the $W^+W^- \to q\bar{q}q\bar{q}$ channel will evolve. Although it is true that the additional data will provide more stringent tests, it is unknown whether the additional sensitivity will actually reveal a discrepancy large enough to justify rejecting any of the remaining viable models. Assuming none of the remaining models are rejected, so that the CR/BE uncertainty remains the same, the projected total uncertainty on $M_W$ at the end of LEP2 operation would be of the order of 35–40 MeV from the LEP combination. If the CR/BE uncertainty can be reduced to less than 15 MeV, it may be possible for the LEP measurement to reach a total uncertainty of 30 MeV.

In spring 2001, the CDF and DØ experiments will start taking data at the Fermilab Tevatron. They anticipate collecting 2–3 $\text{fb}^{-1}$ of data by 2004, which should give a fivefold improvement in the statistical uncertainty of the Tevatron $M_W$ measurement. The systematic uncertainties associated with the energy scale and other detector effects are dominated by the statistics of the $Z$ control samples and are expected to scale accordingly. On the other hand, the systematic uncertainty associated with the $W$ production modeling does not scale directly with statistics and may improve only moderately, to about 20 MeV. The uncertainty from the combined Tevatron $M_W$ determination is expected to be about 30 MeV (69).

On the time scale of the next five years, it is expected that the world average $W$ mass will have a total uncertainty of 20–25 MeV, reducing the present uncertainty by a factor of two. The standard-model constraint on $M_H$ afforded by the $M_W$ measurements alone will be comparable to that afforded by the $\sin\theta_W$ measurements of LEP and SLD, which presently yield an uncertainty of the order of $\Delta M_H = M_H$.

Although these two sets of constraints are correlated through $m_{top}$-dependent corrections, it is still interesting to compare them, since they have differing sensitivities to the various radiative correction terms. A significant improvement to the standard model constraints on $M_H$ requires a more precise determination of $m_{top}$. On the same timescale, the Tevatron experiments are expected to measure $m_{top}$ to 2–3 GeV (69). This improvement should yield constraints on $M_H$ with uncertainties on the order of $\Delta M_H = 0.5 M_H$ [assuming that the fits continue to give a central value of $M_H \sim \mathcal{O}(100)$ GeV] (66).

Looking further ahead, on the timescale of 5–10 years, it is possible that the LHC experiments, CMS and ATLAS, will measure the *W* mass to a precision of 15 MeV and $m_{top}$ to 2 GeV (70). And on the timescale of >10 years, future high-luminosity $e^+e^-$ or $\mu^+\mu^-$ colliders might yield the statistics to envision a <10 MeV measurement of $M_W$ using the threshold method and a <1 GeV measurement of $m_{top}$ (71, 72). If achieved, such precision measurements would yield constraints on $M_H$ with uncertainties of $\mathcal{O}$(1–10) GeV—which we can hope will offer, by that time, a very interesting comparison with a directly measured $M_H$!



## 6. CONCLUSIONS

The mass of the *W* boson has been measured by many experiments at $p\overline{p}$ and $e^+e^-$ colliders. All measurements are in good agreement. The world average of all measurements of the *W* boson mass is 80.398 ± 0.041 GeV. Based on measurements of other parameters, the standard model of the electroweak interactions leads to a prediction of 80.381 ± 0.026 GeV for the mass of the *W* boson, in excellent agreement with the measured value. In the framework of the standard model, this measurement of the *W* boson mass, together with the measurement of the top quark mass, constrains the Higgs boson mass to values below 280 GeV at 90% confidence level. Over the coming decade, a reduction in the uncertainty of the direct measurement of the *W* boson mass by at least a factor of two is expected. As the top quark mass is measured more precisely and the reach of searches for the Higgs boson increases, the comparison of the indirect constraint on the Higgs boson mass and its direct measurement or exclusion region will become one of the most interesting tests of the standard model. This test will for the first time close in on the symmetry-breaking sector of the standard model, about which very little is currently known.

## ACKNOWLEDGMENTS

We would like to thank our colleagues at LEP and the Tevatron, with whom we had the privilege to work on these exciting measurements. In particular, we should like to thank W Carithers, J Goldstein, A Kotwal, M Lancaster, M Narain, H Weerts, J Womersley, N Watson, and D Wood for many helpful comments and suggestions on the manuscript. This work is partially supported by the US Department of

Energy under contracts with Fermi National Accelerator Laboratory and Boston University. One of us (UH) also acknowledges the support of the Alfred P Sloan Foundation.



## LITERATURE CITED


1. Glashow SL. *Nucl. Phys.* A22:579 (1961); Weinberg S. *Phys. Rev. Lett.* 19:1264 (1967); Salam A. In *Elementary Particle Theory*, ed. N Svartholm, p. 367. Stockholm: Almquist & Wiksell (1968)
2. UA1 Collaboration. *Phys. Lett.* B122:103 (1983); UA2 Collaboration. *Phys. Lett.* B122:476 (1983)
3. *Phys. Lett.* B107:306 (1981)
4. UA1 Collaboration. *Z. Phys. C* 47:11 (1990)
5. UA2 Collaboration. *Z. Phys. C* 47:11 (1990)
6. UA2 Collaboration. *Phys. Lett. B* 241:150 (1990)
7. CDF Collaboration. *Nucl. Instrum. Methods A* 271:387 (1988)
8. DØ Collaboration. *Nucl. Instrum. Methods A* 338:185 (1994)
9. Edwards HT. *Annu. Rev. Nucl. Part. Sci.* 35:605 (1985)
10. ALEPH Collaboration. *Nucl. Instrum. Methods A* 294:121 (1990)
11. DELPHI Collaboration. *Nucl. Instrum. Methods A* 303:233 (1991); *Nucl. Instrum. Methods A* 378:57 (1996)
12. L3 Collaboration. *Nucl. Instrum. Methods A* 289:35 (1990); *Nucl. Instrum. Methods A* 349:345 (1994); *Nucl. Instrum. Methods A* 351:300 (1994); *Nucl. Instrum. Methods A* 374:293 (1996); *Nucl. Instrum. Methods A* 381:236 (1996); *Nucl. Instrum. Methods A* 383:342 (1996)
13. OPAL Collaboration. *Nucl. Instrum. Methods A* 305:275 (1991); Anderson BE, et al. *IEEE Trans. Nucl. Sci.* 41:845 (1994); OPAL Collaboration. *Nucl. Instrum. Methods A* 403:326 (1998)
14. Aitchison IJR, Hey AJG. 1989. *Gauge Theories in Particle Physics*. Philadelphia: IOP. 2nd ed. 550 pp.
15. Higgs PW. *Phys. Lett.* 12:132 (1964); *Phys. Rev. Lett.* 135:08 (1964); *Phys. Rev. Lett.* 145:1156 (1966)
16. Montagna G, Nicrosini O, Piccinni F. *Precision Physics at LEP. Riv. Nuovo Cim.* 21:1 (1998)
17. Marciano WJ, Sirlin A. *Phys. Rev. D* 29:945 (1984)
18. UA2 Collaboration. *Phys. Lett. B* 276:365 (1992)
19. DØ Collaboration. *Phys. Rev. Lett.* 75: 1456 (1995); *Phys. Rev. D* 60: 052003 (1999); FERMILAB-PUB-99-171-E
20. DØ Collaboration. *Phys. Rev. Lett.* 80: 3008 (1998); *Phys. Rev. D* 58:092003 (1998)
21. LEP Collaborations ALEPH, DELPHI, L3, OPAL with LEP Energy Working Group and SLD Heavy Flavor Group. CERN-EP/2000-016, p. 5 (2000)
22. CDF Collaboration. *Phys. Rev. Lett.* 75:11 (1995); *Phys. Rev. D* 52:4784 (1995)
23. CDF Collaboration. *Phys. Rev. Lett.* 74: 850 (1995)
24. CDF Collaboration. *Phys. Rev. Lett.* 81: 5754 (1998)
25. Martin AD, Stirling WJ, Roberts RG. *Phys. Rev. D* 50:6734 (1994); *Phys. Rev. D* 51:4756 (1995)
26. Lai HL, et al. *Phys. Rev. D* 51:4763 (1995)
27. Ladinsky GA, Yuan CP. *Phys. Rev. D* 50:4239 (1994)
28. Arnold PB, Reno MH. *Nucl. Phys.* B319:37 (1989), Erratum *Nucl. Phys.* B330:284 (1990); Arnold PB, Kauffman RP. *Nucl. Phys.* B349:381 (1991)

29. Collins J, Soper D. *Nucl. Phys.* B193: 381 (1981), Erratum *Nucl. Phys.* B213:545 (1983); Colions J, Soper D, Sterman G. *Nucl. Phys.* B250:199 (1985)
30. Altarelli G, et al. *Nucl. Phys.* B246:12 (1984)
31. Berends FA, Kleiss R, Revol JP, Vialle JP. *Z. Phys. C* 27:155 (1985); Berends FA, Kleiss R. *Z. Phys. C* 27:365 (1985)
32. Baur U, Berger EL. *Phys. Rev. D* 41:1476 (1990)
33. Baur U, et al. *Phys. Rev. D* 56:140 (1997); Baur U, Keller S, Sakumoto WK. *Phys. Rev. D* 57:199 (1998)
34. UA2 Collaboration. *Phys. Lett.* B276:354 (1992)
35. Harriman PM, Martin AD, Roberts RG, Stirling WJ. *Phys. Rev. D* 42:798 (1990); *Phys. Lett.* B243:421 (1990)
36. CDF Collaboration. *Phys. Rev. Lett.* 65: 2243 (1990); *Phys. Rev. D* 43:2070 (1991)
37. Lancaster M. *Proc. Rencontres de Moriond, XXXIVth.* Gif-sur-Yvette: Ed. Frontieres (1999)
38. CDF Collaboration. *Phys. Rev. D* 50:2966 (1994)
39. Martin AD, Roberts RG, Stirling WJ. *Phys. Rev. D* 37:1161 (1988)
40. Martin AD, Roberts RG, Stirling WJ. *Phys. Lett.* B306:145 (1993), Erratum *Phys. Lett.* B309:492 (1993)
41. Martin AD, Roberts RG, Stirling WJ. *Phys. Lett.* B387:419 (1996)
42. DØ *Phys. Rev. Lett.* 77:3309 (1996); *Phys. Rev. D* 58:012002 (1998)
43. DØ Collaboration. *Phys. Rev. Lett.* 84:222 (2000); FERMILAB PUB-99-237-E
44. Martin AD, Roberts RG, Stirling WJ, Thorne RS. *Eur. Phys. J. C* 4:463 (1998)
45. Kunszt Z, Stirling WJ. In *Physics at LEP2*, ed. G Altarelli, T Sjöstrand, F Zwirner, 1:141–205. Geneva: CERN. 596 pp. (1996)
46. OPAL Collaboration. *Phys. Lett.* B389:416 (1996); DELPHI Collaboration. *Phys. Lett.* B397:158 (1997); L3 Collaboration. *Phys. Lett.* B398:223 (1997); ALEPH Collaboration. *Phys. Lett.* B401:347 (1997)
47. L3 Collaboration. *Phys. Lett.* B413:176 (1997); OPAL Collaboration. *Eur. Phys. J. C* 1:395 (1998); ALEPH Collaboration. *Phys. Lett.* B422: 384 (1998); DELPHI Collaboration. *Eur. Phys. J. C* 2:581 (1998)
48. OPAL Collaboration. *Phys. Lett.* B453:138 (1999); ALEPH Collaboration. *Phys. Lett.* B453:121 (1999); L3 Collaboration. *Phys. Lett.* B454:386 (1999); DELPHI Collaboration. *Phys. Lett.* B46:2410 (1999)
49. Mir L. *W Mass from Fully Hadronic Decays at LEP*; Chierici R.*W Mass from Fully Leptonic and Mixed Decays at LEP.* Both to appear in *Proc. EPS'*99, *Tampere, Finland, 1999*, in press (2000)
50. Beenaker W, Berends FA. See Ref. 45, pp. 81–140
51. Bardin D, et al. *Nucl. Phys. Suppl.* 37B:148 (1994)
52. LEP Energy Working Group, Blondel A, et al. *Eur. Phys. J. C* 11:573 (1999)
53. LEP Collaborations ALEPH, DELPHI, L3, OPAL with LEP Energy Working Group and SLD Heavy Flavor Group. CERN-PPE/97-154, pp. 22–23 (1997)
54. Brown N, Stirling WJ. *Phys. Lett.* B252:657 (1990)
55. LEP Polarisation Collaboration. *Phys. Lett.* B284:431 (1992)
56. Torrence E. *Determination of the LEP Beam Energy.* To appear in *Proc. EPS'99, Tampere, Finland, 1999*, in press (2000)
57. Ballestrero A, et al. *J. Phys.* G24:365 (1998)
58. OPAL Collaboration. *Eur. Phys. J. C* 11:217 (1999)
59. OPAL Collaboration. *Phys. Lett.* B453:153 (1999)
60. LEP Collaborations ALEPH, DELPHI, L3, OPAL with LEP Energy Working Group and SLD Heavy Flavor Group. CERN-EP/2000-016, pp. 29–32 (2000)
61. LEP Collaborations ALEPH, DELPHI, L3, OPAL with LEP Energy Working Group and SLD Heavy Flavor Group. CERN-EP/2000-016 and refs therein.

62. CCFR Collaboration. *Eur. Phys. J. C* 1:509 (1998)
63. McFarland K. *Proc. Rencontres de Moriond, XXXIIIrd.* Gif-sur-Yvette: Ed. Frontieres (1998)
64. CDF Collaboration. 79 1992:1997 (;) DØ Collaboration. *Phys. Rev. D* 58: 052001 (1998); CDF Collaboration. *Phys. Rev. Lett.* 80:2767 (1998); DØ Collaboration. *Phys. Rev. D* 60:052001 (1999); CDF Collaboration. *Phys. Rev. Lett.* 82:271 (1999), Erratum *Phys. Rev. Lett.* 82:2808 (1999)
65. LEP Collaborations ALEPH, DELPHI, L3, OPAL with LEP Energy Working Group and SLD Heavy Flavor Group. CERN-EP/2000- 016, pp. 48–49 (2000)
66. Degrassi G, Gambino P, Sirlin A. *Phys. Lett.* B394:188 (1997); Degrassi G, Gambino P, Passera M, Sirlin A. *Phys. Lett.* B418:209 (1998)
67. Eidelman S, Jegerlehner F. *Z. Phys. C* 67:585 1995
68. Pierce D, Bagger JA, Matchev KT, Zhang RJ. *Nucl. Phys.* B491:3 (1997)
69. Amidei D, Brock R, eds. *Future ElectroWeak Physics at the Fermilab Tevatron: Report of the TeV-2000 Study Group.* FERMILAB-PUB-96-082 (1996)
70. Womersley J, Keller S. *Eur. Phys. J. C* 5:249 (1998)
71. Harris FA, et al, eds. *Physics and Technology of the Next Linear Collider.* SLAC-R-0485 (1996)
72. Barger V, Berger MS, Gunion JF, Han T. *Phys. Rev. D* 56:1714 (1997)

*Annual Review of Nuclear and Particle Science*
*Volume 50, 2000*

# CONTENTS